Radiocarbon Data Reveal Contrasting Sources for Carbon Fractions in Thermokarst Lakes and Rivers of Eastern Canada (Nunavik, Quebec)

Regina Gonzalez Moguel[1], Adrian M. Bass[2], Mark H Garnett[3], Martin Pilote[4,6], Benjamin Keenan[1], Alex Matveev[5,6], Peter M. J. Douglas[1]

1. McGill University, Earth and Planetary Sciences; Geotop Research Centre
2. University of Glasgow, School of Geographical and Earth Sciences
3. NEIF Radiocarbon Laboratory
4. Environment and Climate Change Canada
5. Concordia University, Department of Geography and Environment
6. Centre d'études nordiques, Université Laval

Corresponding authors: Regina Gonzalez Moguel (regina.gonzalezmoguel@mail.mcgill.ca), Peter Douglas (peter.douglas@mcgill.ca)

Key points:

- Soil type influences the age of carbon fractions, with a greater contribution of millennia-aged carbon in peatland systems.
- In peatland systems diffusive CH_4 and CO_2 mostly contain centennial-old carbon but ebullition CH_4 largely contains millennia-old carbon.
- In peatland systems dissolved and particulate carbon fractions contained older carbon in winter, but CH_4 ^{14}C age did not vary seasonally.

This article has been accepted for publication and undergone full peer review but has not been through the copyediting, typesetting, pagination and proofreading process, which may lead to differences between this version and the Version of Record. Please cite this article as doi: 10.1029/2020JG005938.

Abstract

Greenhouse gas (GHG) emissions from permafrost organic carbon decomposition in lakes and rivers can accelerate global warming. We used radiocarbon (^{14}C) measurements to determine the predominant sources of dissolved organic carbon (DOC), particulate organic carbon (POC), dissolved inorganic carbon (DIC), and methane (CH_4) in five thermokarst lakes and three rivers in an area of widespread permafrost degradation in Northern Quebec to assess contributions from thawing permafrost and other old carbon (fixed before CE 1950) reservoirs. We compared emission pathways (dissolved gas and ebullition), seasons (summer and winter), and surface soil type (mineral and peat soils). Modern carbon (fixed after CE 1950) was the dominant source of DOC, DIC, and CH_4 of non-peatland aquatic systems, while POC and sediment carbon were predominantly fixed in the last millennia. In the peatland systems, modern and permafrost carbon were important sources of DOC, lake DIC, lake ebullition CO_2, and lake dissolved CH_4. In contrast, POC, lake ebullition CH_4, and river DIC were dominated by millennial-old carbon. In winter, the ^{14}C age of DOC, DIC, and POC in the peatland lakes increased, but the ^{14}C age of dissolved CH_4 did not change. Our results point to a clearly older overall carbon source for ebullition CH_4 relative to dissolved CH_4 in the peatland lakes, but not the non-peatland lakes. The younger ages of diffusive CH_4 and DIC relative to DOC and POC in all lakes suggest that recent primary productivity strongly influences the large total lake CH_4 emissions in this area, as diffusion fluxes greatly exceed ebullition fluxes.

Plain language summary

Permafrost thaw could expose organic carbon to microbial decomposition to methane (CH_4) and carbon dioxide (CO_2) in aquatic systems and accelerate global warming, but the magnitude of this feedback is highly uncertain. We used carbon-14 and a carbon-14 mixing model to determine the main sources of different aquatic carbon pools in five lakes and three rivers in a region of widespread permafrost degradation and to assess the permafrost contribution to these pools. We found that the carbon sources varied between lakes and rivers in peatlands and in mineral soils. The peatlands systems contained a large proportion of organic carbon sourced by permafrost carbon and older carbon sources such as deep peat or marine carbon, but the dissolved CH_4 and dissolved inorganic carbon (DIC), including CO_2, had a larger contribution of modern carbon than the organic carbon. The exception was the lake CH_4 from bubbles and river DIC, which contained a large amount of old carbon sources. In contrast, the mineral soil carbon pools were mainly sourced by contemporary carbon. The results imply that while permafrost carbon is likely incorporated to the aquatic organic carbon, modern carbon from recent primary productivity is the largest source of CH_4 and CO_2.

1. Introduction

Warming-induced permafrost thaw enables the transport of large stocks of previously frozen soil organic carbon through aquatic systems as dissolved organic carbon (DOC) and particulate organic carbon (POC), and its subsequent microbial mineralization to methane (CH_4) and carbon dioxide (CO_2) (Kling et al., 1991; Schuur et al., 2015). Permafrost-derived CH_4 and CO_2 represent a net input of carbon to the atmosphere and a positive feedback to climate change, but there is a large uncertainty on the extent of this feedback as variations in landscape relief, permafrost extent, ice content, composition and degree of processing of permafrost material, vegetation, and hydrological factors all influence how aquatic system carbon-cycling responds to thaw (Tank et al., 2020). Radiocarbon (^{14}C) measurements are used to estimate the contribution of permafrost carbon to DOC, POC, and CH_4 and CO_2, as the storage of soil carbon in permafrost for hundreds to thousands of years results in distinct ^{14}C ages (Estop-Aragonés et al., 2020, Dean et al., 2018, Elder et al., 2018, 2019). The ^{14}C content of the carbon fraction indicates the weighted sum of the ^{14}C signals of the carbon sources, which means that the approximate relative contribution from each carbon source can be estimated with a mass balance if the ^{14}C content of the endmembers is known.

Analyses of ^{14}C-DOC and ^{14}C-POC have shown that previously frozen organic carbon is exported from thawed permafrost soils and transported and mineralized in Arctic rivers (Estop-Aragonés et al., 2020). In these studies, aged soil organic carbon represented most of the river POC, while modern carbon constituted the majority of river DOC except for a few sites where labile and highly depleted ^{14}C-DOC was present (Guo and Macdonald, 2006; Guo et al., 2007; Lamoureux and Lafreniere, 2014; Mann et al., 2015, Spencer et al., 2015, Wang et al., 2018; Wild et al., 2019). Despite the potential for DOC and POC to transport permafrost organic carbon across

the Arctic and Subarctic landscapes and increase potential mineralization in aquatic systems, there are very few studies analyzing ^{14}C of DOC and POC in lakes (Dean et al., 2018).

Thermokarst lakes are widespread across the circumpolar north (Olefeldt et al., 2016) and are sites of intense microbial activity that favors the degradation of organic carbon to CH_4 and CO_2, which are typically emitted through diffusive, ebullition (bubbles), and plant-mediated fluxes (Bastviken et al., 2004). Radiocarbon age measurements of CH_4 and CO_2 from thermokarst lakes span wide ranges (modern to 50 000 yrs BP), varying greatly between different geological settings and emissions pathways (Estop-Aragonés et al., 2020). Ebullition CH_4 has frequently been shown to transport permafrost organic carbon to the atmosphere, with the specific $^{14}CH_4$ ages depending on the age of local soil organic carbon deposits (Zimov, et al. 1997; Walter et al., 2006; Walter et al., 2016; Bouchard et al., 2015). In contrast, more limited datasets have found dissolved $^{14}CH_4$ and $^{14}CO_2$ ages to be younger relative to local soil organic carbon deposits, implying that modern carbon is largely incorporated to CH_4 and CO_2 diffusive fluxes (Elder et al., 2018, 2019; Dean et al., 2018). Overall, most ^{14}C data from thermokarst systems is from a few sites in Alaska, Eastern Siberia, and Western Canada (Estop-Aragonés et al., 2020), with relatively limited datasets from Eastern Canada (Bouchard et al., 2015; Matveev et al., 2016, 2018; Preskeinis et al., 2021). Only two of these studies directly compared diffusive and ebullition CH_4 fluxes in the same site (Elder et al., 2019; Preskeinis et al., 2021)

Rapid warming and a widespread decrease in permafrost area and degradation of permafrost landforms has been recorded in Northern Quebec (Eastern Canada) in the last 30 years (Smith et al., 2010; Laberge and Payette, 1995; Vallée and Payette, 2007; Bouchard et al., 2014). The collapse of peat permafrost mounds (*palsas*) and mineral permafrost mounds (*lithalsas*) has led to the formation of thermokarst lakes and the subsequent release of CH_4 and CO_2. Particularly

high CH_4 and CO_2 diffusive fluxes have been measured in thermokarst lakes in the southernmost permafrost border, where degradation is more advanced (Matveev et al., 2016, 2018). However, it is not clear if the higher diffusive fluxes in more southerly lakes is due to the enhanced mineralization of permafrost carbon, or alternately to increased primary productivity and bioavailable plant-derived carbon (Wang and Roulet, 2017).

In this study, we aimed to determine what the predominant carbon sources of DOC, DIC, POC, and CH_4 are in five thermokarst lakes and three rivers in the sporadic permafrost region of Northern Quebec. We specifically examined whether carbon sources differed between: (1) lakes and rivers in different soil types (peatland and non-peatland), (2) the ice-free and ice-covered seasons, and (3) dissolved and ebullition CH_4 and CO_2. To address these questions, we measured the ^{14}C content, $\delta^{13}C$, and concentration of: ebullition CH_4 and CO_2, dissolved CH_4, DIC, DOC, POC, and surficial sediments from three palsa-associated lakes and two lithalsa-associated lakes in summer; dissolved CH_4, DIC, DOC and POC from the palsa lakes in winter; and DIC, DOC, and POC in two non-peatland rivers (sampled in summer) and one peatland river (sampled in winter). We also used a ^{14}C end-member mixing model to estimate the relative contribution of potential carbon sources to DOC, POC, DIC, and CH_4 fluxes in the different lakes and rivers.

2. Study Sites

All the sampled lakes and rivers are located in the sporadic permafrost region near the Hudson Bay, within 15 km of Kuujjuarapik-Whapmagoostui (K-W) in Nunavik, Quebec, Canada (Figure 1). The Tyrell Sea submerged this area after regional deglaciation roughly after around 8000 yrs BP (Hillaire-Marcel, 1976). The end of the Tyrell sea transgression, resulting from isostatic uplift, initiated the deposition of organic soils and the widespread formation of peatlands

over marine clays after around 5700 cal. yrs BP, or approximately 5000 yrs BP (Arlen-Pouliot and Bhiry, 2005). Although the time of permafrost aggradation in the sampling sites is not completely constrained, it has been inferred from stratigraphic, microfossil, and ^{14}C analyses that permafrost development and the formation of palsas and lithalsas in the Great Whale River area initiated as early as 1600 yrs BP, and probably intensified during the Little Ice Age (500–100 yrs BP) (Bhiry and Robert, 2006; Arlen-Pouliot and Bhiry, 2005; Fillon et al., 2014). After the Little Ice Age, the degradation of permafrost and collapse of palsas and lithalsas resulted in the formation of thermokarst lakes and an increase of the vegetation cover in the area (Arlen-Pouliot & Bhiry, 2005; Bouchard et al., 2014), a process that continues to the present. Regional vegetation is classified as forest tundra, with different areas dominated by grasses, lichen, shrubs, and spruce forests (Bhiry et al., 2011), as well as sedges in peatlands (Wang & Roulet, 2017).

2.1 Palsa lakes

We sampled three palsa-associated thermokarst lakes located southeast of K-W in a peatland adjacent to the Sasapimakwananisikw River (known as the SAS2 peatland) in two consecutive summers (August 2018 and 2019) and one winter (February 2019; Figure 1). Permafrost in the SAS2 peatland underlies the palsa mounds, but there is a rapid transition to permafrost-free soil towards the bog and lakes (Vincent et al., 2017). The area close to the palsas is vegetated by deciduous and ericaceous shrubs (*Betula glandulosa, Kalmia polifolia, Ledum groenlandicum*), the permafrost-free soil by peat moss (*Sphaghnum* spp.), and sedges (*Carex* spp.) are dominant close to the lakes (Wang & Roulet, 2017).

The three sampled lakes -SAS2A, SAS2B, and SAS2C- are less than 2.8 meters deep and have surface areas between 115 and 230 m^2 (Matveev et al., 2020). All lakes stratify in summer,

becoming anoxic below 0.5–1 meter (Figure 1; Figure S1). The measured summer diffusive fluxes in these lakes are high relative to other thermokarst lakes in the region, ranging 1–10 mmol CH_4 m^{-2} day^{-1} and 40–242 mmol CO_2 m^{-2} day^{-1} (Matveev et al., 2016). In contrast, ebullition fluxes range 0.01–0.5 mmol CH_4 m^{-2} day^{-1} and from less than 0.001 to 0.1 mmol CO_2 m^{-2} day^{-1} (Matveev et al., 2016). Ice covers the lakes from mid-October to May, and the entire water column becomes anoxic during this period (Deshpande et al., 2015; Matveev et al., 2016, 2019).

2.2 Lithalsa lakes

We sampled two lithalsa-associated thermokarst lakes located northeast of K-W in a once-glaciated valley adjacent to the Kwakwatanikapistikw River (KWK valley) in two consecutive summers (August 2018 and 2019; Figure 1). Due to the difficulty of site access, we were not able to sample in winter. Bouchard et al. (2014) calculated that the permafrost surface cover in the KWK valley decreased by 96% from 1959 to 2006, leaving only one visible lithalsa. In 2019, we observed that the remaining lithalsa had disappeared. The permafrost degradation in the valley resulted in the increase of vegetation cover and growth of shrubs (*Salix* spp., *Alnus crispa, Myrica gale*), mosses (*Sphaghnum* spp.), and herbaceous plants such as sedges (*Carex* spp.) between the lakes (Bouchard et al., 2014).

The two sampled lakes – KWK1 and KWK12 – are less than 2.8 meters deep and have areas of 390 and 480 m^2 (Matveev et al., 2020). Both lakes stratify in summer, developing anoxic conditions below 1.5 meters (Laurion et al., 2010). Measured diffusive fluxes in these lakes are lower than in the SAS2 lakes, averaging 0.47 ± 0.33 mmol CH_4 m^{-2} day^{-1} and 20.2 ± 7.1 mmol CO_2 m^{-2} day^{-1} (Matveev et al., 2018). Ebullition fluxes average 0.016 mmol CH_4 m^{-2} day^{-1} and 0.06 mmol CO_2 m^{-2} day^{-1} (Matveev et al., 2018).

2.3 Rivers

We sampled the Sasapimakwananisikw River (SAS River) in winter (February 2019) from two locations adjacent to each other (55°12'35.9"N, 77°41'05.1"W). The SAS River runs Southeast to Northwest and its course is parallel to the Great Whale River (Figure 1). The river drains several peatlands, including SAS2, before flowing into the Hudson Bay, approximately 1 km SW of the mouth of the Great Whale River. To our knowledge, there are no studies exploring the limnological characteristics of the SAS River. In summer (August 2019), we sampled two smaller rivers in catchments that do not drain peatlands: a small tributary of the SAS River (55°13'53.4"N, 77°41'22.6"W) and a small river that flows parallel to the Great Whale River (55°15'05.2"N, 77°44'26.1"W). Due to logistical and access constraints, we were only able to sample the two non-peatland rivers in the summer of 2019, and the SAS River in winter of 2019.

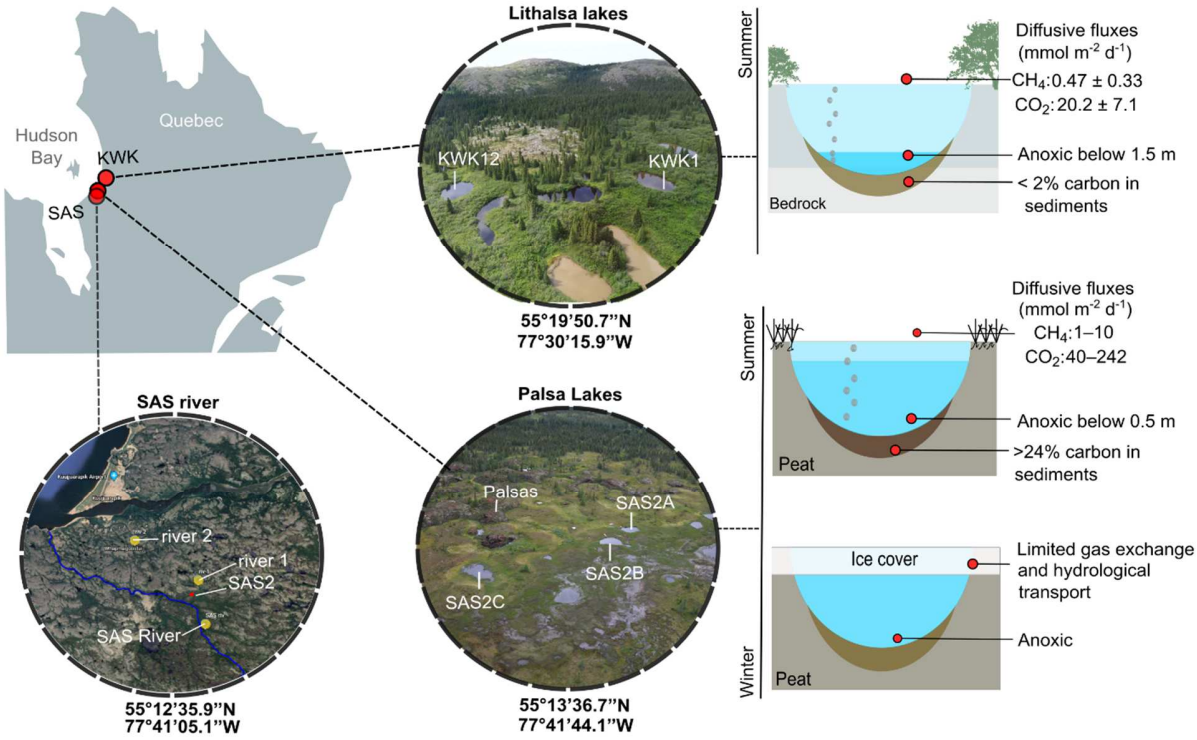

Figure 1. Location, aerial photographs, and schematics of the KWK lithalsa lakes (summer) and SAS2 palsa lakes (summer and winter) showing the diffusive fluxes magnitude (Matveev et al., 2016, 2018) and oxygenation patterns (Figure S1); and satellite image of the rivers sampling locations in yellow (Google Earth, 2020).

3. Methods

3.1 Sample collection

3.1.1 Ebullition gas (bubbles)

We placed one to three gas-tight submerged funnels, described in Matveev et al. (2016), attached to a 140 mL syringe close to the center of the lakes and fixed them with a rope staked to the lake shore to limit movement. Five to eight days later, we recorded the collected gas volume and transferred the gas from the syringe to an evacuated 120 mL vial sealed with a crimped butyl stopper. We stored the vials at room temperature until analysis. In winter 2019, the SAS2 palsa lakes were completely covered with ice and ebullition was not observed and therefore not collected. In summer 2019, bubbles were only collected in the SAS2 palsa lakes.

3.1.2 Dissolved methane

To collect dissolved CH_4, we used the technique described in Garnett et al. (2016). We added 400–600 mL of water from a depth of 1–1.5 m below the surface to a 1.1 L bottle, shook the bottle for three minutes, and analyzed the headspace concentration using a Sensit Technologies SENSIT PMD portable methane detector. We used the concentration of CH_4 in the headspace to calculate the volume of water needed to produce 5–10 mL of CH_4. We then pumped the required volume of water (2–14 liters) into an 'accordion water carrier' using a Proactive Environmental ALEXIS peristaltic pump or a hand pump. In the winter, we drilled through the ice before pumping

the water. Then, we used a syringe to add 1–2 L of ambient air to the accordion and shook for three minutes. Lastly, we transferred the accordion headspace to a 6 L pre-evacuated canister (Silonite Canister, Entech Instruments, USA), using a hydrophobic filter to prevent water from entering the canister.

3.1.3 Water sampling

We collected water samples for DIC, DOC, and POC analyses from 1 to 1.5 meters below the lake surface using the peristaltic pump or the hand pump. We filtered the water with a 0.7 μm (47 mm diameter) pre-baked glass fiber filter and transferred it to a pre-baked and acid washed 1 L vial (for ^{14}C analysis) and to three 40 mL pre-cleaned borosilicate amber vials with extra septa (for concentration and $\delta^{13}C$ analyses). We freeze-dried the filters and kept them in the fridge at 4° C until analysis. In winter, we transported the collected water to the research station in 3 L acid rinsed Nalgene bottles, and performed the filtration the same day. All water samples were stored at 4° C with no fixing agent added and were delivered for analysis within 15 days of collection. It is possible that during these 15 days a small portion of DOC was respired to DIC, resulting in DIC ages looking more similar than DOC ages.

We did not collect dissolved CO_2 but we assumed that that DIC and dissolved CO_2 have a similar ^{14}C signal (Mayorga et al., 2005), because carbon exchange within the DIC pool is rapid (Zhang et al., 1995) and any isotopic fractionation effects are corrected when normalizing the radiocarbon results. Additionally, the relatively low pH of the lakes at the sampled depth, ranging from approximately 5 to 6.5, indicates that the predominant DIC species is dissolved CO_2 in most lakes (Figure S1).

3.1.4 Sediments

In summer 2018, we collected sediments from close to the center of the lakes using a Wildco hand corer. In the SAS2 palsa lakes, roughly the first 10–15 cm of the core were composed of organic rich lacustrine mud (gyttja). Below the gyttja layer the cores consisted of clay. These sediment samples represent a spectrum of depositional ages that are not constrained as we do not know the accumulation rates of the sites. In the KWK lithalsa lakes, only about 4–6 cm of the core was gyttja, and the rest was clay. Previous sediment analyses in these lakes measured ^{14}C ages of up to 1000 cal. yrs BP in the upper sediments (gyttja) and determined that most of the upper sediment was deposited in the last 150 years based on ^{210}Pb and ^{137}Cs measurements (Bouchard et al., 2011). In both sites we sampled and homogenized the gyttja from the cores and discarded the clay, as we aimed to estimate an average ^{14}C age of the shallow sediments that could be contributing to ebullition CH_4 and CO_2 production . We freeze-dried and stored the sediments at 4 °C until analysis.

3.2 Concentration and $\delta^{13}C$ analysis

3.2.1 Dissolved and ebullition CH_4 and CO_2

The ebullition CH_4 and CO_2 concentrations were measured alongside two standards (5000 ppm CO_2 and 2000 ppm CH_4) at McGill University using a Shimadzu 2014 gas chromatograph (GC) with a flame ionization detector (FID) and a methanizer. The 2019 ebullition $\delta^{13}C$-CH_4 and $\delta^{13}C$-CO_2 were measured in the Ján Veizer Stable Isotope Laboratory (University of Ottawa, Canada) using a GC Isolink system interfaced via a Conflo 4 to a Delta V Isotope Ratio Mass spectrometer and normalized using the international standards USGS HCG-1, USGS HCG-2, and USGS HCG-3 (U.S. Geological Survey Hydrocarbon Gas). The dissolved $\delta^{13}C$-CH_4 and 2018 ebullition $\delta^{13}C$-CH_4 were measured at the NEIF Radiocarbon Laboratory (East Kilbride, UK), using a dual inlet stable isotope mass spectrometer (Thermo Fisher Delta V) in the pre-prepared

sample. To calculate the concentration of dissolved CH_4, we divided the mass of CH_4, calculated from the volume of CH_4 recovered from the canister using the ideal gas law, by the volume of water (in L) that we degassed in the accordion water carrier. We did not calculate the dissolved CH_4 concentrations in winter 2019, as the formation of ice in the accordion system led to unreliable water volume estimations.

3.2.2 DIC and DOC

The concentration and $\delta^{13}C$ of DOC and DIC in the water samples were measured in the Ján Veizer Stable Isotope Laboratory (University of Ottawa, Canada) as described in Lalonde et al. (2014). The samples in the 40 mL amber vials and two standard solutions (KHP and sucrose) were loaded into a carousel. Then, an aliquot was injected into a reaction chamber and acidified with 5% H_3PO_4. The released gas was carried using ultra-pure helium. Water was removed and the CO_2 (DIC) concentration in the gas measured by a nondispersive infrared sensor (NDIR). Subsequently, the $\delta^{13}C$-CO_2 (DIC) was measured using a Thermo Finnigan DeltaPlus XP isotope ratio mass spectrometer (IRMS). After the inorganic carbon was removed, a persulfate reagent was added to the aliquot to oxidize the organic carbon (DOC) to CO_2, which was measured for concentration and $\delta^{13}C$ as described above. The 2σ analytical precision is 0.5 mg L^{-1} for the concentration, and ±0.2 ‰ for the isotopes.

3.2.3 POC and sediments

The concentration and $\delta^{13}C$ of the filters and the sediments were measured in the GEOTOP Light Stable Isotope Geochemistry Laboratory (Montreal, Canada). Samples were weighed in tin cups and analyzed alongside two internal reference standards with a Micromass model Isoprime 100 Isotope Ratio Mass Spectrometer coupled to an Elementar Vario MicroCube elemental

analyzer in continuous flow mode. A third reference material was analyzed to assess the uncertainty of the normalization. The results were normalized to the NBS19-LSVEC scale and expressed in delta units against VPDB. Analytical uncertainty (2σ) was <±0.2‰. To calculate POC concentration, we multiplied the measured carbon fraction in the filter (%) by the total weight of the sample (mg), which was calculated as the difference of the dry weight of the filter before and after sampling. Then, we divided the carbon mass in the filter (mg) by the volume of water filtered (L). Water volumes, and therefore concentrations, were only recorded for summer 2019.

Because the filters and sediment were not acidified prior to analysis, we used two residual filter and sediment samples to test whether acidification (24 hours with 36% HCl) changed the concentration and $\delta^{13}C$ of POC and sediment carbon. The differences in $\delta^{13}C$ between the acidified and unacidified sediments (collected from the surface organic rich layer) and filters were within the range of analytical uncertainty (2σ ~ ±0.2‰). Therefore we reported the $\delta^{13}C$ of unacidified samples as the $\delta^{13}C$ of sedimentary organic carbon and POC. In the case of concentration, the difference between acidified and unacidified filters (0.9–2 mg L^{-1}) and sediments (0.7–1.13%) were both outside the uncertainty range. Therefore, we report the concentrations of unacidified samples as the concentrations of total sedimentary carbon and total particulate carbon.

3.3 ^{14}C sample preparation and analysis

The DOC, DIC, POC, sediments, and 2019 ebullition samples were prepared and analyzed in the A.E. Lalonde AMS Laboratory (University of Ottawa, Canada) according to the methods described in Crann et al. (2017), Murseli et al. (2019), and Pack et al. (2015) . For DIC, phosphoric acid (85%) was added to the sample in a pre-baked borosilicate bottle at 60°C and the resulting gas was cryogenically separated in a breakseal. Then, for DOC, around 8 mL of sodium persulfate

solution (400 g/L) and 1 mL of $AgNO_3$ catalyst (0.5 N) were added to the same sample, the mixture was heated to 95 °C for at least one hour, and the resulting gas was again separated in a breakseal. The POC and sediment samples were treated with an acid wash to remove carbonates (HCl, 1N, 80°C, 30 min), freeze-dried, weighed in tin cups, combusted to CO_2 using a Thermo Flash 1112 elemental analyzer (EA), and the CO_2 was cryogenically separated in a breakseal.

To separate the CH_4 from the ebullition samples, the sample was transferred to a combustion line with an ultra-zero gas carrier at a flow of 10 mL/min, where CO_2 was separated cryogenically, CO was oxidized to CO_2 in a 300°C oven with CuO and separated cryogenically. Then, CH_4 was combusted to CO_2 in a 975°C tube furnace packed with CuO and stored in a pre-baked breakseal. To separate the CO_2, the sample was extracted and flushed 10 times at 200 ml/min with Helium, CO_2 was trapped cryogenically on a U-trap packed with Silver wool, then transferred to a vacuum line for cryogenic purification with a -80°C ethanol slurry to remove water and other non-condensable gases, and lastly transferred to a pre-baked breakseal. All the breakseals, containing grains of silvered cobaltous/cobaltic oxide, were baked at 200°C to remove sulfur and halogens. The CO_2 in the breakseals was reduced to graphite in the presence of Fe-H. ^{14}C of the resulting graphite was analyzed on a 3MV tandem accelerator mass spectrometer (AMS). The results were background-corrected.

The 2018 ebullition samples (CO_2 and CH_4) and all the dissolved gas samples (CH_4) were prepared at the NEIF Radiocarbon Laboratory (East Kilbride, UK) using the methods described in Garnett et al. (2012). In the case of CH_4 analysis, CO_2 was removed from the sample using soda lime and zeolite molecular sieve. The CH_4 was then combusted on 950°C Pt/Al beads to CO_2. The resulting CO_2 was separated cryogenically and reduced to graphite using Fe/Zn reduction. For ebullition CO_2 analysis, CO_2 was separated cryogenically and reduced to graphite as described

above. The ^{14}C analyses of these samples were performed at the Scottish Universities Environmental Research Centre (SUERC) AMS laboratory, or the Keck Carbon Cycle AMS Facility (University of California, Irvine, USA).

In all cases the results were normalized to $\delta^{13}C$ VPDB‰ = 25 using the IRMS-measured $^{13}C/^{12}C$ ratios in samples analyzed in the SUERC AMS Laboratory and using the AMS-measured $^{13}C/^{12}C$ ratios in samples analyzed in the Keck Carbon Cycle AMS Laboratory and A.E. Lalonde AMS Laboratory. All the results were reported as Fraction Modern Carbon (FMC) and conventional radiocarbon ages (years BP, where 0 BP = AD 1950) at the ± 1σ level. In this document, we report the radiocarbon (^{14}C) age averages, but include the FMC averages where the age is modern (FMC > 1.0). In data that contain both modern and pre-1850 ages, we report the range of ^{14}C ages, rounded to the closest hundred.

3.4 Isotope separation factor ε_c calculation

We calculated the ebullition and dissolved isotope separation factor $\boldsymbol{\varepsilon_c}$ for ebullition and dissolved CO_2 and CH_4 using the equation $\varepsilon_c = \delta^{13}C_{CO2} - \delta^{13}C_{CH4}$, after Whiticar (1999). To derive the dissolved $\delta^{13}C\text{-}CO_2$ from $\delta^{13}C$-DIC, we first calculated the distribution of the CO_2 (dissolved), HCO_3^-, and CO_3^{2-} species at a depth of 1.5 meters using the pH values and DIC concentrations at that depth. The winter pH and temperature values were obtained from Matveev et al. (2019, 2020). Then, we used a mass balance equation and the isotope fractionation factors ($\alpha_{A\text{-}B} = R_A/R_B$), obtained from Zhang et al. (1995), between pure CO_2 (gas) and CO_2 (dissolved), bicarbonate (HCO_3^-), and carbonate (CO_3^{2-}) to calculate the dissolved $\delta^{13}C\text{-}CO_2$. The complete calculations are available in the Supporting Information.

3.5 Carbon source ^{14}C mixing model

We used IsoSource to calculate the ranges of possible contributions from five carbon sources to the mean FMC carbon of DOC, POC, DIC, dissolved CH_4, and ebullition CO_2 in the lithalsa and palsa thermokarst lakes, as well as DOC, POC, and DIC in the rivers. IsoSource is a software that generates every possible combination of source mixing proportions that sums to 100%, in 2% increments. The predicted mixture signature of every solution is compared to the observed mixed signature, and only the ones within the tolerance level are considered a feasible solution (Phillips and Greg, 2003). We used the standard deviation of the measurements of each carbon fraction (~0.04) as the tolerance value.

We performed the mixing model with five sources, using the mid-point FMC value of each source: (1) carbon from marine sediments deposited during the Tyrell sea transgression from around 8000 to 5000 yrs BP (FMC: 0.453); (2) "deep" carbon from peat deposition after the Tyrell sea retreat around 5000 yrs BP and until widespread permafrost formation around 500 yrs BP (FMC: 0.738), (3) carbon preserved in soils after permafrost development in the area during the Little Ice Age from around 500 yrs BP until thaw began around 100 yrs BP (FMC: 0.964), (4) carbon fixed after permafrost thaw and corresponding to the post-bomb period, calculated as the integrated annual average of atmospheric $^{14}CO_2$ from 1950–2012 by Elder et al. (2018) (FMC: 1.221); and (5) carbon from recent photosynthesis, from 2013 to 2018, which was also defined by Elder et al. (2018) (FMC: 1.031). No fossil carbon sources are known in this area, as there are no known deposits of fossil fuels or significant pre-Holocene sedimentary units.

4. Results

4.1 DOC and POC

DOC was consistently 100–2800 ^{14}C years younger and 0.5–7.0 ‰ more $\delta^{13}C$ enriched than POC in all lakes and rivers and for all the seasons sampled (Figure 2A). The lower $\delta^{13}C$-POC relative to DOC was much more pronounced in the lithalsa lakes. The ^{14}C age difference between DOC and POC resulted in a larger estimated contribution of old carbon sources (i.e. "deep" and marine carbon) to POC relative to DOC by the mixing model (Figure 3). Where comparison was possible, the concentration of the particulate carbon, ranging 1–2 mg L^{-1}, was approximately one order of magnitude lower than the DOC concentrations, which ranged 7–32 mg L^{-1}.

DOC and POC from lakes and rivers associated with peatlands were older and contained a larger proportion of old carbon sources than lakes and rivers not associated with peatlands (Figures 2A and 3). In the non-peatland lakes and rivers, DOC was modern (FMC: ~1.07), with a relatively large proportion of carbon fixed during the bomb period (Figure 3), while ^{14}C-POC ages ranged 100–800 yrs BP. In comparison, the ^{14}C-DOC and ^{14}C-POC from peatland lakes and rivers dated up to one-millennia old (300–1500 yrs BP) and up to three millennia old (900–3100 yrs BP), respectively. DOC concentrations also varied between sites (Table S1), with the palsa lakes having a higher average DOC concentration (21.0 ± 4.7 mg L^{-1} in summer and 29.2 ± 3.8 mg L^{-1} in winter) than the lithalsa lakes (8.7 ± 1.5 mg L^{-1}), non-peatland rivers (12.1 ± 3.8 mg L^{-1}), and the SAS river (8.1 ± 0.3 mg L^{-1}).

In winter, the palsa lakes ^{14}C-DOC and ^{14}C-POC ages, and DOC concentrations increased (Figure 2A and 2B). The results of the mixing model indicated a greater contribution of older carbon sources to DOC and POC in this season (Figure 3). This change was especially pronounced in POC, which was mostly sourced by marine carbon and to a lesser extent by "deep" carbon in the SAS2 lakes and SAS river (Figure 3).

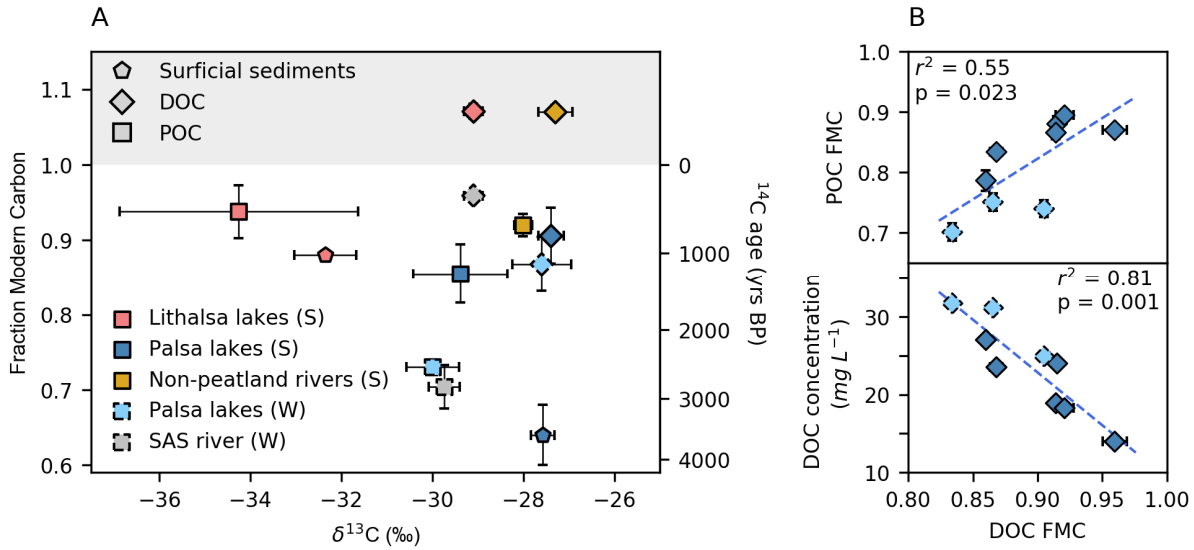

Figure 2. (A) $\delta^{13}C$ and ^{14}C content of DOC (diamonds), POC (squares), and sediment organic carbon (pentagons) by site in summer (S) and winter (W). The gray area represents modern carbon (fixed after CE 1950). (B) In the SAS2 palsa lakes there were significant linear relationships ($p<0.05$) between the ^{14}C-DOC and ^{14}C-POC and DOC concentration.

4.2 Sedimentary Carbon

The concentration, $\delta^{13}C$, and ^{14}C ages of the surficial sedimentary carbon varied between the lithalsa and palsa lakes (Figure 2A, Table S1). The collected sediment from the palsa lakes had a high carbon content that averaged 29.7 ± 6.2 % and ^{14}C ages that ranged three to four millennia (3200–4300 yrs BP), while in the lithalsa lakes the carbon content was low, averaging 2.4 ± 1.6 %, and yielded a ^{14}C age of 1000 yrs BP.

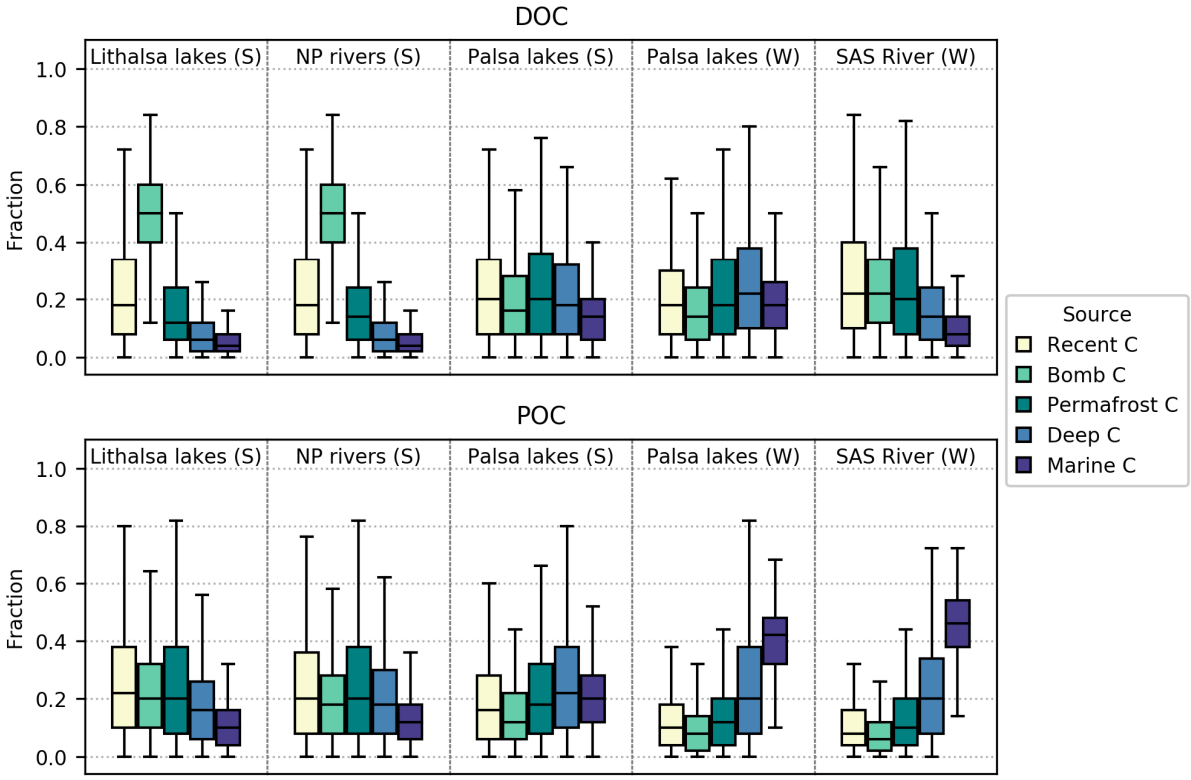

Figure 3. Potential contributions from five carbon sources to the ^{14}C content of DOC and POC by site in summer (S) and winter (W). The boxplots show the median, the first quartile (Q1) and third quartile (Q3). The range represents the range of the feasible solutions.

4.3 CH_4

The $\delta^{13}C$-CH_4 and ^{14}C-CH_4 ages differed between the lithalsa and palsa lakes and between the dissolved and ebullition pools (Figure 4A). In the lithalsa lakes, we found low dissolved CH_4 concentrations (sampled above the hypolimnion), ranging from less than 0.003 ppm to 0.21 ppm. When analysis was possible, ^{14}C-CH_4 was primarily modern (FMC: 1.01 ± 0.04), implying a large proportion of carbon fixed during the bomb period (Figure 5), and $\delta^{13}C$-CH_4 was relatively enriched (-54.7 ± 0.1‰), which probably reflects extensive CH_4 oxidation in these lakes (Figure

S2). On the other hand, dissolved ^{14}C-CH_4 ages in the palsa lakes (sampled in the hypolimnion) ranged from modern to 600 yrs BP and did not significantly change between summer and winter (Figure 4A), implying predominant source contributions from recent carbon and centennial-aged permafrost carbon in both seasons (Figure 5). In summer, the concentration of dissolved CH_4 (7.7 ± 2.3 ppm) in these lakes showed a positive linear relationship with DOC (Figure 4C).

The concentration of ebullition CH_4 varied greatly between samples (0.4–30%), and even between replicates from the same site. Comparison of ^{14}C ages between ebullition and dissolved CH_4 revealed a much larger difference in the palsa lakes than in the lithalsa lakes (Figure 2A). Ebullition ^{14}C-CH_4 in the lithalsa lakes was modern (FMC: 1.05) and similarly to dissolved CH_4, there was a large contribution of carbon fixed during the bomb period (Figure 5). In the palsa lakes, ebullition CH_4 was approximately one millennium old (1000–1800 yrs BP), and contained a much larger proportion of deep peat and marine carbon compared to dissolved CH_4 (Figure 5).

In addition to the source variability, the isotope separation factors ε_c ($\varepsilon_c = \delta^{13}C_{CO2} - \delta^{13}C_{CH4}$) indicated variable CH_4 production pathways between the palsa and the lithalsa lakes (Figure S2). In the palsa lakes, ebullition and dissolved CH_4 showed ε_c values spanning both hydrogenotrophic and acetotrophic ranges (47–57‰) in the summer, but the ε_c value of dissolved CH_4 increased to 54–60 ‰ in the winter, suggesting a shift of the methane production pathway towards increased hydrogenotrophic methanogenesis (Whiticar, 1999). In the lithalsa lakes, the highly depleted ebullition $\delta^{13}C$-CH_4 (~-71‰) suggested a higher production of CH_4 by hydrogenotrophic methanogenesis, or potentially the utilization of ^{13}C depleted substrates to produce CH_4, as suggested by the low $\delta^{13}C$ values of POC and sedimentary OC in these lakes.

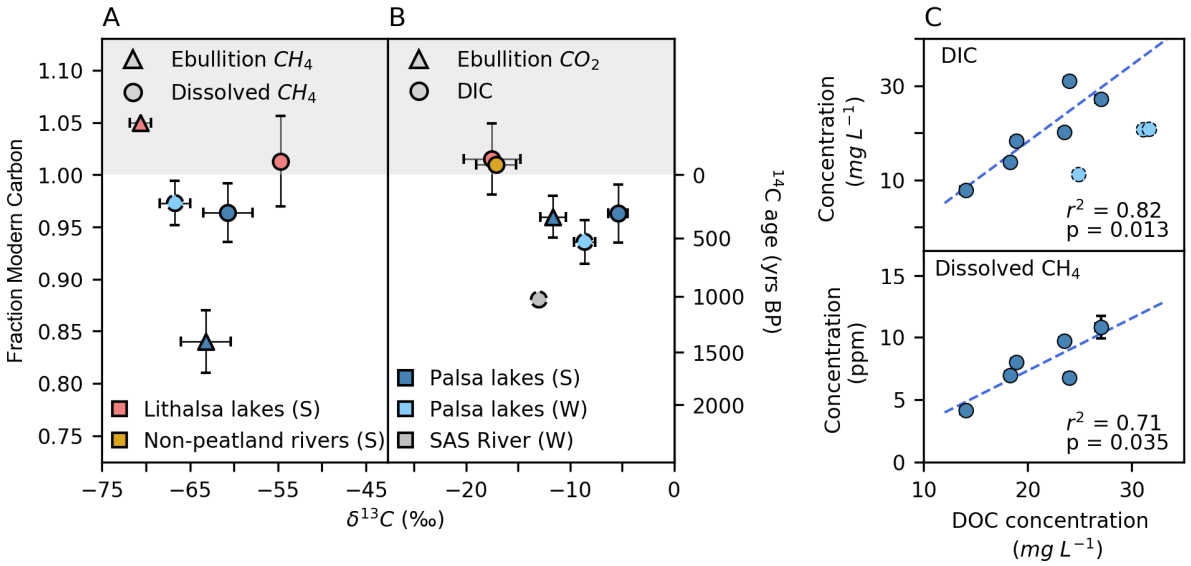

Figure 4. $\delta^{13}C$ and ^{14}C content of (A) dissolved and ebullition CH_4 and (B) ebullition CO_2 and DIC by site. The gray area represents modern carbon (fixed after CE 1950). (C) In the SAS2 palsa lakes, the DIC and dissolved CH_4 concentration increase linearly with DOC concentration ($p>0.05$) in summer (S), but not in winter (W).

4.4 Ebullition CO_2 and DIC

The ^{14}C-DIC ages and source contributions varied across sites (Figure 4B and Figure 5). The SAS river yielded the oldest ages (1000–1100 yrs BP), with the largest contributions from deep carbon and permafrost carbon (Figure 5). In the palsa lakes, the summer ^{14}C-DIC ranged from modern to 600 yrs BP (excluding one outlier), indicating that the main sources were recent carbon and centennial-aged permafrost carbon (Figure 5). In the winter, DIC in these lakes shifted to slightly older ages (400–800 yrs BP) (Figure 4), implying a larger contribution of older carbon sources in this season (Figure 5). The youngest DIC ages were found in the lithalsa lakes and non-

peatland rivers (modern to 300 yrs BP), and like dissolved CH_4, DIC in these systems had a large contribution of bomb carbon and to a lesser extent recent carbon (Figure 5).

The DIC concentration and δ^{13}C-DIC also varied across sites (Figure 4, Table S1): palsa lakes had the highest DIC concentrations (19.0 ± 7.4 mg L^{-1}), which showed a linear relationship with DOC concentrations in summer (Figure 4C), and more positive δ^{13}C-DIC (-6.5 ± 1.8‰). Lower DIC concentrations (5.6 ± 1.2 mg L^{-1}) and δ^{13}C-DIC (-13.0 ± 0.2‰) were observed in the SAS river. The lithalsa lakes and non-peatland rivers showed the lowest DIC concentration (2.3 ± 1.4 mg L^{-1}) and more negative δ^{13}C-DIC (-17.3 ± 2.3‰).

Compared to ebullition CH_4, the concentration of CO_2 in bubbles was lower and less variable (0.2–3%); and was below the ^{13}C and ^{14}C analytical limit in the samples from lithalsa lakes. In the palsa lakes, ebullition ^{14}C-CO_2 (modern to 500 yrs BP) was younger than ebullition ^{14}C-CH_4 , but within the age range of ^{14}C-DIC (Figure 4B). In addition, the mixing model showed a similar source contribution between ebullition CO_2 and DIC in these lakes, both containing a larger proportion of recent and bomb carbon compared to ebullition CH_4 (Figure 5).

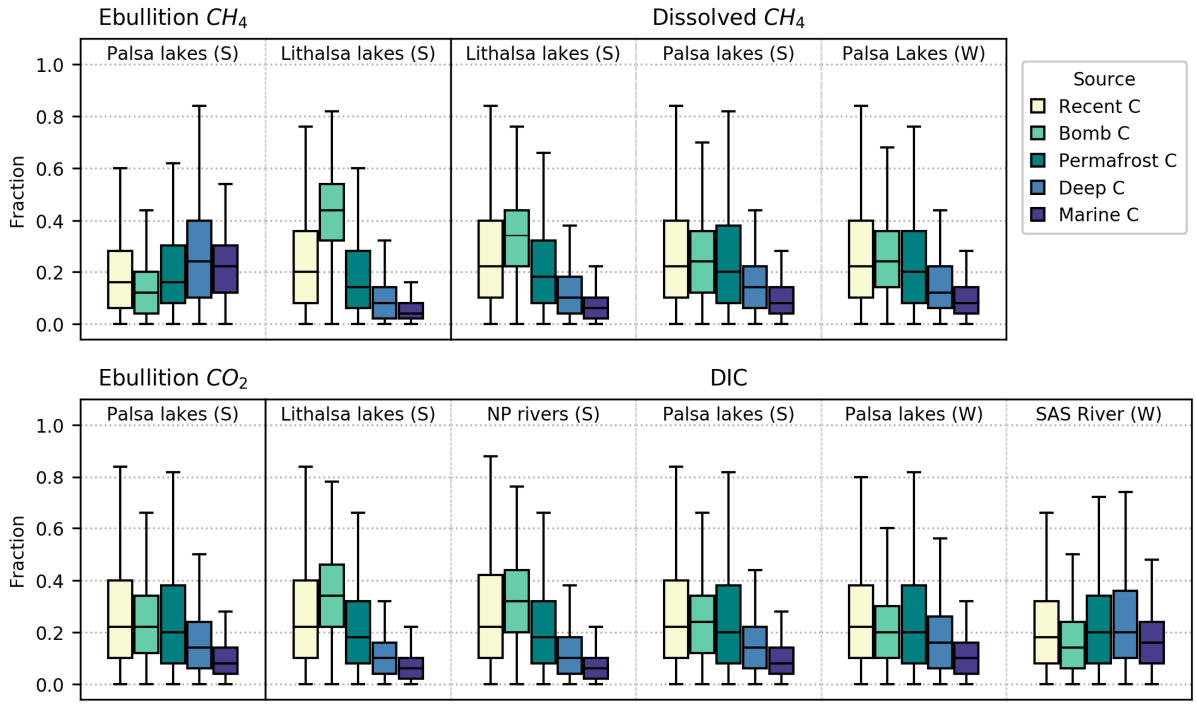

Figure 5. Potential contributions from five carbon sources to the ^{14}C content of ebullition CH_4 and CO_2, dissolved CH_4, and DIC by site in summer (S) and winter (W). The boxplots show the median, the first quartile (Q1) and third quartile (Q3). The range represents the range of the feasible solutions.

5. Discussion

5.1 Difference in carbon sources between lake and river soil type

Soil type had a clear influence on the ages and source contributions of lake and river DOC. Centennial-aged permafrost carbon and modern carbon were the largest DOC sources in the SAS2 palsa lakes (Figure 3), emphasizing the influence of aquatic or terrestrial primary productivity and recent peat accumulation in the organic carbon export in these systems. In comparison, modern carbon strongly dominated DOC in the lithalsa lakes and non-peatland rivers (Figure 3), with a particularly large proportion of carbon fixed during the bomb period. This suggests that terrigenous

carbon sources cycling on decadal timescales, such as shallow soil organic matter, likely predominated over carbon from autochthonous primary productivity, which would have a contemporary ^{14}C signature. These results are consistent with evidence from Arctic rivers, which shows that DOC does transport some pre-modern organic carbon, but it is dominantly derived from young carbon reservoirs (Dean et al., 2020; Guo et al., 2007; Raymond et al., 2007; Wild et al., 2019).

POC represented a small fraction of the total organic carbon in the lakes and rivers, but old carbon sources constituted a much larger portion of POC compared to DOC in all of our sites. Measurements of ^{14}C-POC in other circum-Arctic rivers have shown that old carbon is transported mainly in the POC fraction, likely eroded or exported from permafrost soils (Guo et al., 2007; Lamoureux and Lafreniere, 2014; Wild et al., 2019), and as a consequence the POC ages in rivers is a function of regional or local soil age (Estop-Aragonés et al., 2020). The observed similarity between the POC ages in the non-peatland rivers and the KWK lithalsa lakes, and between the SAS2 palsa lakes and SAS river, could be related to the export of POC to the lakes and rivers from surrounding soils and the greater abundance of old carbon preserved in peat soils.

A notable feature of our data was that $\delta^{13}C$-POC was 2–3‰ lower than $\delta^{13}C$-DOC and surficial sedimentary carbon in lakes, and especially the lithalsa lakes, but not in the rivers. We speculate that particle-attached microbial communities are an important component of POC in lakes, causing the low $\delta^{13}C$-POC, as methanogenic and methanotrophic communities are highly abundant in the SAS2 and KWK lakes (Crevecoeur et al., 2015, 2016, 2017) and uptake ^{12}C preferentially, resulting in their biomass being more isotopically depleted in ^{13}C than the substrates (Fuchs et al., 1979; Summons et al., 1998). However, this particle-attached microbial biomass does not appear to be exported to the rivers we sampled.

The ^{14}C age distribution of CH_4 and DIC was also influenced by the soil type. As with DOC and POC, CH_4 and DIC consistently exhibited younger ^{14}C ages in the non-peatland lakes and rivers (Figure 4A). The strong bomb carbon input observed in non-peatland lake and river DOC (Figure 3) was also apparent in lithalsa lake CH_4, both in ebullition and dissolved fractions, and non-peatland lake and river DIC. These results suggest a strong influence of terrestrial soil carbon that is cycled on decadal timescales in the total CH_4 and CO_2 emissions of non-peatland systems. In contrast, the palsa lakes dissolved CH_4 and DIC contained inputs of centennial aged permafrost carbon, and the palsa lakes ebullition CH_4 and SAS river DIC contained inputs from even older carbon sources. The difference in CH_4 and DIC between the peatland and non-peatland lakes is broadly consistent with previous studies (Elder et al., 2018; Dean et al., 2020) that have found that the geological substrate and soil type exerts a strong influence on the age of carbon emitted from lacustrine CH_4 and CO_2 fluxes.

Overall, it is clear that in our study area the peatland lakes and rivers contain a much larger fraction of carbon from pre-modern reservoirs than the non-peatland aquatic systems. This difference may be partly a result of the more advanced stage of permafrost degradation in the KWK valley if permafrost carbon reservoirs have already been largely mobilized. This difference is also likely a function of the much larger reservoirs of old carbon in peat soils, and the fact that this carbon is decomposed more slowly than carbon in mineral soils, regardless of the presence of permafrost (Frolking et al., 2001). This result emphasizes the likely importance of peatlands as a landscape feature when considering the cycling and emission of old carbon in regions undergoing permafrost thaw (Hugelius et al., 2020).

5.2 Sources of CH_4 and CO_2 in different emission pathways

Variations in the contributions of old organic carbon to CH_4 between the dissolved and ebullition pathways were only observed in the palsa lakes, where the ebullition CH_4 had a substantially larger contribution of older sources compared to dissolved CH_4 (Figure 5). Modern and permafrost-aged carbon were the primary sources of dissolved CH_4 and DIC in the palsa lakes, suggesting that the peatland or lacustrine primary productivity strongly influences CH_4 and CO_2 diffusive emissions in these lakes. The close relationship between DOC, and DIC and CH_4 summer concentrations suggests that DOC fuels both DIC and dissolved CH_4 microbial production either in the surrounding peatland, shallow sediments, or in the water column. This is also supported by the inference from carbon isotope separation values that dissolved CH_4 in summer is largely produced through the acetotrophic pathway (McCalley et al., 2014). The younger ages of CH_4 and DIC relative to DOC could be explained by reduced reactivity of older DOC carbon (Douglas et al., 2020), implying that dissolved CH_4 is produced from a more labile component of DOC with relatively young ages. We suggest that peat organic matter deposited before permafrost development (i.e. deposits older than 500 yrs BP) has undergone a greater degree of microbial decomposition before being frozen than carbon accumulated after ~500 yrs BP, resulting in these old carbon deposits being more recalcitrant to microbial communities.

By contrast, the ebullition ^{14}C-CH_4 ages in the palsa lakes reflected the ^{14}C age of the organic carbon in the surficial sediment, probably due to the production of bubbles in the sediment pore waters. The high hydrostatic pressure and osmotic and capillary forces in the sediments slow the diffusion of methane and favor the accumulation of methane in bubbles (Stepanenko et al., 2011), which are released when the pore pressure exceeds a certain threshold. The relatively young age of ebullition CH_4 in the lithalsa lakes (Figure 4A) probably reflects the young overall age of sediments in these lakes (Figure 2A), whereas in the palsa lakes older ^{14}C ages in sediments are

leading to the release of old carbon in ebullition CH_4. In turn, the differences in sediment age are likely a function of the difference in carbon sources to POC and DOC in these lakes. In both lakes sediment OC is similar in its ^{14}C age distribution to POC, and in the palsa lakes input of old carbon in the form of POC may be driving the observed contribution of old carbon reservoirs to ebullition CH_4. In general, our results from the SAS2 palsa ebullition CH_4 support previous reports of ^{14}C-CH_4 ages in thermokarst lakes that have demonstrated the key role of bubbles for emitting old soil organic carbon to the atmosphere in the form of CH_4 and CO_2 (Bouchard et al., 2015; Elder et al., 2019; Walter et al., 2016).

Compared to ebullition CH_4, the contribution of older carbon sources to ebullition CO_2 of the palsa lakes was limited. The higher solubility of CO_2 in water and the incorporation of younger CO_2 during the formation and rise of the bubbles to the surface could explain why the ebullition CO_2 was younger and less concentrated than CH_4 but within the range of radiocarbon ages of DIC. Similar age discrepancies between ebullition CH_4 and CO_2 have been observed in some sites in Canada and Alaska (Elder et al., 2019; Matveev et al., 2016; Bouchard et al., 2015), although other thermokarst lakes in Eastern Canada show the opposite trend, with older CO_2 ebullition ages (Bouchard et al., 2015; Matveev et al., 2018). The mechanism for the reversed ^{14}C age differences between ebullition CH_4 and CO_2 in different lakes remains unclear. Even though our results showed that carbon fixed during the bomb period strongly dominated ebullition CH_4 in the lithalsa lakes, previous studies have measured millennial-old ebullition CO_2 from lithalsa lakes in sites undergoing thaw or recently thawed (Matveev et al., 2018), implying that there is potential for old carbon release specifically through CO_2 ebullition fluxes in lithalsa lakes.

Overall, for both the palsa and lithalsa lakes diffusive fluxes represent much larger CH_4 and CO_2 emissions than ebullition fluxes (Matveev et al., 2016, 2018). The substantial contribution

of modern carbon sources to dissolved CH_4 and DIC in all lakes (Figure 5) suggest that these fluxes are largely fueled by recently fixed carbon probably from aquatic or terrestrial primary productivity, despite the presence of older organic carbon in both these aquatic systems. This could suggest that the increase of vegetation growth in permafrost free areas, which increases the input of labile DOC from plant exudates into aquatic environments, will strongly influence diffusive CO_2 and CH_4 emissions from thermokarst lakes of Nunavik in Northern Quebec. These results are similar to other studies highlighting that diffusive CH_4 and CO_2 fluxes from lakes incorporate large proportions of modern carbon (Cooper et al., 2017; Dean et al., 2020; Elder et al., 2019).

5.3 Seasonal variations of carbon sources in the palsa lakes

The seasonal variation of ^{14}C-DOC and ^{14}C-POC in the palsa lakes indicated a larger contribution of older carbon sources in the ice-cover season. This increase was more pronounced in POC, which was dominated by old carbon sources in winter (Figure 3). Results from previous studies comparing the DOC or POC seasonal variation in aquatic systems have shown that progressively older DOC is exported from spring to winter, probably due to an increase in active layer depth (Dean et al., 2020; Wild et al., 2019). In the palsa lakes, the input of DOC from deeper and older peat layers that remained unfrozen for all or part of the ice cover season while the upper and younger peat layers were frozen could potentially explain the seasonal changes. This change in carbon input might be coupled with a slower rate of DOC decomposition at colder temperatures, which could explain the simultaneous increase of DOC concentrations and ^{14}C ages in the ice-cover season. Moreover, changes in the redox conditions in these lakes could result in the remobilization of DOC and POC from the sediments, for example, through the dissolution of organic carbon complexed with iron under reducing conditions (Gonsior et al., 2013; Skoog and Arias-Esquivel, 2009). Previous studies looking at 16r RNA in the SAS2A lake showed there is

an increased potential for reducing metabolisms in winter, including iron reducers (Vigneron et al., 2019).

Despite the higher abundance of older DOC and POC in the ice-cover season, the dissolved ^{14}C-CH_4 age did not vary seasonally. In contrast, ^{14}C-DIC was on average older in the ice-cover season. We hypothesized that the older DOC added to the water column in the ice cover season is more recalcitrant and less available to methanogens. Alternatively, it may contain limited quantities of substrates involved in methanogenesis (e.g. acetate) but larger quantities of substrates metabolized by other CO_2 producing metabolisms including fermentative bacteria. The apparent shift to a greater prevalence of hydrogenotrophic methanogenesis in the ice-cover, based on ε_C, season may have also contributed to a lack of seasonal change in dissolved ^{14}C-CH_4 ages, since DIC in the ice cover season has an average ^{14}C age that is younger than that of DOC (Figure 4).

These results contrasted with results from a previous study comparing lake dissolved ^{14}C-CH_4 and ^{14}C-CO_2 ages in the ice-free and ice-cover season (Elder et al., 2019). This study found that in a Yedoma thermokarst lake in Alaska, dissolved CH_4 and CO_2 were both significantly older in the winter, at least in part due to the accumulation and dissolution of bubbles under the ice, which lowered the ^{14}C age of dissolved CH_4 (Elder et al., 2019). In the SAS2 palsa lakes, we did not observe evidence of ebullition in the winter. There were no visible openings in the ice or bubble accumulation in the surface that could have been released by the drilling of ice and missed by our sampling procedure. We argue that the ebullition ^{14}C-CH_4 signal is probably not detectable in the winter dissolved ^{14}C-CH_4 data, since ice-free season ebullition fluxes are one order of magnitude less than dissolved fluxes (Matveev et al., 2017). It is also plausible that the cooling of sediments in the winter results in a slower production of bubbles in these lakes (Wik et al., 2014).

Overall, our data point to intriguing seasonal differences in the source and age of carbon cycled in the palsa lakes. The mechanisms responsible for this variability are unclear, but it would be interesting to observe whether similar patterns occur in other permafrost environments. Regardless, this seasonal change in carbon cycling does not appear to have a strong effect on the source and age of carbon that is converted to GHG, and in particular CH_4. This, along with the general finding of a relatively young dissolved ^{14}C age, implies that the mobilization of old carbon reservoirs into aquatic environments does not necessarily lead to this carbon being released to the atmosphere. This is generally consistent with other studies implying a limited role of old carbon reservoirs in GHG emissions in some areas of permafrost thaw (Elder et al., 2018; Cooper et al., 2017; Dean et al., 2020).

6. Conclusions

We identified potential sources of DOC, POC, CH_4, and DIC in lakes and rivers near Northern Quebec's permafrost southern limit to evaluate if the increasing GHG emissions are fueled by permafrost carbon or other carbon reservoirs. We found that the soil type strongly influenced the age of the organic carbon and GHG present in the lakes and rivers, but in all sites POC contained a larger proportion of old carbon sources than DOC. The non-peatland lakes and rivers contained primarily modern DOC, DIC, and both dissolved and ebullition CH_4, in particular ^{14}C enriched carbon fixed during the bomb period.

The peatland-associated systems contained from modern to millennia-aged DOC and POC, likely including a significant contribution from permafrost carbon. In winter, both DOC and POC contained a larger proportion of old carbon sources, most likely deep peat carbon and marine sediments. Dissolved CH_4 and DIC were younger than DOC and POC and were sourced mainly by modern and centennial-aged permafrost-aged carbon in both summer and winter, implying that

increased amounts of old organic carbon input to the lakes was not readily metabolized by methanogens. In contrast, the millennial-aged ebullition CH_4 in the palsa lakes and DIC in the SAS river indicated larger contribution of old carbon from deep peat and marine sediments. Whether this millennia aged DIC carbon in the SAS river will be transported to the atmosphere as CO_2 is not clear, as CO_2 fluxes from this river are not well constrained, and their magnitude relative to fluxes from the lakes remains unclear.

Overall, these results indicated that carbon fixed in the past few centuries is the primary source of diffusive CH_4 and CO_2 fluxes in all lakes and all seasons, which in this region greatly exceed ebullition fluxes that contain a greater proportion of millennial-aged carbon. Therefore, even though there is a clear presence of millennial-aged carbon in the landscape, and specifically within these aquatic ecosystems in the form of POC and sediments, this carbon is not strongly contributing to the large observed greenhouse gas fluxes. However, given the relatively recent timing of permafrost formation in this landscape, it is likely that destabilization of permafrost is contributing to greenhouse gas emissions, specifically in the peatland lakes.

Data availability statement

The concentration, $\delta^{13}C$, and ^{14}C data used to support the results of this research are available through the open repository Figshare (DOI: 10.6084/m9.figshare.13114433)

Acknowledgements

This research was funded by the National Science and Engineering Research Council of Canada Discovery Grant Northern Research Supplement (NSERC DG 03902), the Trottier Institute for Science and Public Policy Fellowship, The Fonds de Recherche de Québec Nature et Technologie New Researcher Grant (NC-253022), the NERC Radiocarbon Facility NRCF010001

(allocation number 2128.1018), and the Concordia CUPFA PD Grant 2019. We thank Dr. Isabelle Laurion and Dr. Warwick Vincent for their scientific inputs on the study area; the Centre d'études nordiques, Stephanie Arnold, Richard Petagumskum, Sydney Aruda, and Patrick Lacerte for their support in the field; the UQAM-GEOTOP Light Stable Isotope Geochemistry Laboratory, the University of Ottawa Lalonde Radiocarbon Laboratory, the University of Ottawa Ján Veizer Laboratory, Thi Bu Hao, and Mike Dalva for their sample analysis support; and Robert Bogue for his assistance with Python coding. Last, we acknowledge the Mexican National Council of Science and Technology (CONACYT) for partially sponsoring Regina Gonzalez Moguel PhD studies.

References

Arlen-Pouliot, Y., & Bhiry, N. (2005). Palaeoecology of a palsa and a filled thermokarst pond in a permafrost peatland, subarctic Québec, Canada. *The Holocene*, *15*(3), 408-419. https://doi.org/10.1191/0959683605hl818rp

Bastviken, D., J. Cole, M. Pace, and L. Tranvik (2004), Methane emissions from lakes: Dependence of lake characteristics, two regional assessments, and a global estimate. *Global Biogeochem. Cycles*, *18*(4). https://doi:10.1029/2004GB002238.

Bhiry, N., & Robert, É. C. (2006). Reconstruction of changes in vegetation and trophic conditions of a palsa in a permafrost peatland, subarctic Québec, Canada. Écoscience, 13(1), 56-65. https://doi.org/10.2980/1195-6860(2006)13[56:ROCIVA]2.0.CO;2

Bhiry, N., Delwaide, A., Allard, M., Bégin, Y., Filion, L., Lavoie, M., ... & Vincent, W. F. (2011). Environmental change in the Great Whale River region, Hudson Bay: Five decades of multidisciplinary research by Centre d'études nordiques (CEN). Ecoscience, 18(3), 182-203. https://doi.org/10.2980/18-3-3469

Bouchard F, Francus P, Pienitz R, Laurion I (2011). Sedimentology and geochemistry of thermokarst ponds in discontinuous permafrost, subarctic Quebec, Canada. *Journal of Geophysical Research –Biogeosciences, 116*(G00M04). http://dx.doi.org/10.1029/2011JG001675

Bouchard, F., Francus, P., Pienitz, R., Laurion, I., & Feyte, S. (2014). Subarctic thermokarst ponds: Investigating recent landscape evolution and sediment dynamics in thawed permafrost of northern Québec (Canada). *Arctic, Antarctic, and Alpine Research*, *46*(1), 251-271. https://doi.org/10.1657/1938-4246-46.1.251

Bouchard, F., Laurion, I., Preskienis, V., Fortier, D., Xu, X., & Whiticar, M. J. (2015). Modern to millennium-old greenhouse gases emitted from ponds and lakes of the Eastern Canadian Arctic (Bylot Island, Nunavut). *Biogeosciences*, *12*, 7279–7298. https://doi.org/10.5194/bg-12-7279-2015

Cooper, M. D., Estop-Aragonés, C., Fisher, J. P., Thierry, A., Garnett, M. H., Charman, D. J., ... & Wolfe, S. A. (2017). Limited contribution of permafrost carbon to methane release from thawing peatlands. *Nature Climate Change*, 7(7), 507-511. https://doi.org/10.1038/nclimate3328

Crann, C. A., Murseli, S., St-Jean, G., Zhao, X., Clark, I. D., & Kieser, W. E. (2017). First status report on radiocarbon sample preparation techniques at the AE Lalonde AMS Laboratory (Ottawa, Canada). *Radiocarbon, 59*(3), 695-704. doi:10.1017/RDC.2016.55

Crevecoeur, S., Vincent, W. F., Comte, J., & Lovejoy, C. (2015). Bacterial community structure across environmental gradients in permafrost thaw ponds: methanotroph-rich ecosystems. *Frontiers in microbiology*, *6*, 192. https://doi.org/10.3389/fmicb.2015.00192

Crevecoeur, S., Vincent, W. F., & Lovejoy, C. (2016). Environmental selection of planktonic methanogens in permafrost thaw ponds. *Scientific reports*, *6*(1), 1-10. https://doi.org/10.1038/srep31312

Crevecoeur, S., Vincent, W. F., Comte, J., Matveev, A., & Lovejoy, C. (2017). Diversity and potential activity of methanotrophs in high methane-emitting permafrost thaw ponds. *PloS one*, *12*(11). https://doi.org/10.1038/srep31312

Dean, J. F., Van Der Velde, Y., Garnett, M. H., Dinsmore, K. J., Baxter, R., Lessels, J. S., … Billett, M. F. (2018). Abundant pre-industrial carbon detected in Canadian Arctic headwaters: Implications for the permafrost carbon feedback. *Environmental Research* Letters, 13(3). https://doi.org/10.1088/1748-9326/aaa1fe

Dean, J. F., Meisel, O. H., Rosco, M. M., Marchesini, L. B., Garnett, M. H., Lenderink, H., ... & Röckmann, T. (2020). East Siberian Arctic inland waters emit mostly contemporary carbon. *Nature communications, 11*(1), 1-10. https://doi.org/10.1038/s41467-020-15511-6

Deshpande, B. N., MacIntyre, S., Matveev, A., & Vincent, W. F. (2015). Oxygen dynamics in permafrost thaw lakes: Anaerobic bioreactors in the Canadian subarctic. *Limnology and Oceanography*, *60*(5), 1656-1670. https://doi.org/10.1002/lno.10126

Douglas, P. M. J., Gonzalez Moguel, R., Walter Anthony, K. M., Wik, M., Crill, P. M., Dawson, K. S., … Sessions, A. L. (2020). Clumped Isotopes Link Older Carbon Substrates With Slower Rates of Methanogenesis in Northern Lakes. *Geophysical Research Letters*, *47*(6), 1–10. https://doi.org/10.1029/2019GL086756

Elder, C. D., Xu, X., Walker, J., Schnell, J. L., Hinkel, K. M., Townsend-Small, A., … Czimczik, C. I. (2018). Greenhouse gas emissions from diverse Arctic Alaskan lakes are dominated by young carbon. *Nature Climate Change*, *8*(February). https://doi.org/10.1038/s41558-017-0066-9

Elder, C. D., Schweiger, M., Lam, B., Crook, E. D., Xu, X., Walker, J., … Czimczik, C. I. (2019). Seasonal Sources of Whole-Lake CH4 and CO2 Emissions From Interior Alaskan Thermokarst Lakes. *Journal of Geophysical Research: Biogeosciences*, *124*(5), 1209–1229. https://doi.org/10.1029/2018JG004735

Estop□Aragonés, C., Olefeldt, D., Abbott, B. W., Chanton, J. P., Czimczik, C. I., Dean, J. F., et al. (2020). Assessing the potential for mobilization of old soil carbon after permafrost thaw: A synthesis of 14C measurements from the northern permafrost region. Global Biogeochemical Cycles, 34, e2020GB006672. https://doi.org/10.1029/2020GB006672

Fillion, M. È., Bhiry, N., & Touazi, M. (2014). Differential development of two palsa fields in a peatland located near Whapmagoostui-Kuujjuarapik, Northern Quebec, Canada. *Arctic, antarctic, and alpine research*, *46*(1), 40-54. https://doi.org/10.1657/1938-4246-46.1.40

Frolking, S., Roulet, N. T., Moore, T. R., Richard, P. J., Lavoie, M., & Muller, S. D. (2001). Modeling northern peatland decomposition and peat accumulation. *Ecosystems*, 4(5), 479-498. DOI: 10.1007/s10021-001-0105-1

Fuchs, G., Thauer, R., Ziegler, H., & Stichler, W. (1979). Carbon isotope fractionation by Methanobacterium thermoautotrophicum. *Archives of Microbiology*, *120*(2), 135-139.https://doi.org/10.1007/BF00409099

Garnett, M. H., Hardie, S. M. L., & Murray, C. (2012). Radiocarbon analysis of methane emitted from the surface of a raised peat bog. *Soil Biology and Biochemistry*, *50*, 158-163. https://doi.org/10.1016/j.soilbio.2012.03.018

Garnett, M. H., Gulliver, P., & Billett, M. F. (2016). A rapid method to collect methane from peatland streams for radiocarbon analysis. *Ecohydrology*. https://doi.org/10.1002/eco.1617

Gonsior, M., Schmitt-Kopplin, P., & Bastviken, D. (2013). Depth-dependent molecular composition and photo-reactivity of dissolved organic matter in a boreal lake under winter and summer conditions. *Biogeosciences*, *10*(11), 6945-6956. https://doi.org/10.5194/bg-10-6945-2013

Guo, L. and Macdonald, R.W., 2006. Seasonal fluxes and age of particulate organic carbon exported from Arctic catchments impacted by localized permafrost slope disturbances. *Global Biogeochemical Cycles*, *20*(2).

Guo, L., Ping, C. L., & Macdonald, R. W. (2007). Mobilization pathways of organic carbon from permafrost to arctic rivers in a changing climate. *Geophysical Research Letters*, *34*(13), 1–5. https://doi.org/10.1029/2007GL030689

Hillaire-Marcel, C. (1976). La déglaciation et le relèvement isostatique sur la côte est de la baie d'Hudson. Cahiers de géographie du Québec, 20 (50), 185–220.https://doi.org/10.7202/021319ar

Hugelius, G., Loisel, J., Chadburn, S., Jackson, R. B., Jones, M., MacDonald, G., ... & Treat, C. (2020). Large stocks of peatland carbon and nitrogen are vulnerable to permafrost thaw. *Proceedings of the National Academy of Sciences*, *117*(34), 20438-20446.

Kling, G. W., Kipphut, G. W., & Miller, M. C. (1991). Arctic lakes and streams as gas conduits to the atmosphere: implications for tundra carbon budgets. *Science*, *251*(4991), 298-301.

Laberge, M. J., & Payette, S. (1995). Long-term monitoring of permafrost change in a palsa peatland in northern Quebec, Canada: 1983–1993. *Arctic and Alpine Research*, *27*(2), 167-171. https://doi.org/10.1080/00040851.1995.12003110

Lalonde, K., Middlestead, P., & Gélinas, Y. (2014). Automation of 13C/12C ratio measurement for freshwater and seawater DOC using high temperature combustion. *Limnology and Oceanography: Methods, 12*(12), 816-829. https://doi.org/10.4319/lom.2014.12.816

Lamoureux, S.F. and Lafreniere, M.J., 2014. Seasonal fluxes and age of particulate organic carbon exported from Arctic catchments impacted by localized permafrost slope disturbances. *Environmental Research Letters*, *9*(4), p.045002.

Laurion, I., Vincent, W. F., MacIntyre, S., Retamal, L., Dupont, C., Francus, P., & Pienitz, R. (2010). Variability in greenhouse gas emissions from permafrost thaw ponds. *Limnology and Oceanography*, *55*(1), 115-133. https://doi.org/10.4319/lo.2010.55.1.0115

Mann, P. J., Eglinton, T. I., McIntyre, C. P., Zimov, N., Davydova, A., Vonk, J. E., … Spencer, R. G. M. (2015). Utilization of ancient permafrost carbon in headwaters of Arctic fluvial networks. *Nature Communications*, *6*, 7856. https://doi.org/10.1038/ncomms8856

Matveev, A., Laurion, I., Deshpande, B. N., Bhiry, N., & Vincent, W. F. (2016). High methane emissions from thermokarst lakes in subarctic peatlands. *Limnology and Oceanography*, *61*(S1), S150-S164. https://doi.org/10.1002/lno.10311

Matveev, A., Laurion, I., & Vincent, W. F. (2018). Methane and carbon dioxide emissions from thermokarst lakes on mineral soils. *Arctic Science*, *4*(4), 584-604. https://doi.org/10.1139/as-2017-0047

Matveev, A., Laurion, I., & Vincent, W. F. (2019). Winter Accumulation of Methane and its Variable Timing of Release from Thermokarst Lakes in Subarctic Peatlands. *Journal of Geophysical Research: Biogeosciences*, *124*(11), 3521-3535. https://doi.org/10.1029/2019JG005078

Matveev, A., Laurion, I., Deshpande, B.N., Vincent, W.F. 2020. Concentrations of dissolved methane, carbon dioxide and oxygen in thermokarst lakes and ponds in palsa peatlands, northern Québec, Canada, v. 1.100000 (2012-2017). Nordicana D48, doi: 10.5885/45588CE-5A12A84DFAAF4D36.

Mayorga, E., Aufdenkampe, A. K., Masiello, C. A., Krusche, A. V., Hedges, J. I., Quay, P. D., ... & Brown, T. A. (2005). Young organic matter as a source of carbon dioxide outgassing from Amazonian rivers. Nature, 436(7050), 538-541. https://doi.org/10.1038/nature03880

McCalley, C. K., Woodcroft, B. J., Hodgkins, S. B., Wehr, R. A., Kim, E. H., Mondav, R., … Saleska, S. R. (2014). Methane dynamics regulated by microbial community response to permafrost thaw. *Nature*, *514*(7253), 478–481. https://doi.org/10.1038/nature13798

Murseli, S., Middlestead, P., St-Jean, G., Zhao, X., Jean, C., Crann, C. A., ... & Clark, I. D. (2019). The Preparation of Water (DIC, DOC) and Gas (CO 2, CH 4) Samples for Radiocarbon Analysis at AEL-AMS, Ottawa, Canada. *Radiocarbon*, *61*(5), 1563-1571. http://doi.org/10.1017/RDC.2019.14

Olefeldt, D., Goswami, S., Grosse, G., Hayes, D., Hugelius, G., Kuhry, P., … Turetsky, M. R. (2016). Circumpolar distribution and carbon storage of thermokarst landscapes. *Nature Communications*, *7*(1), 13043. https://doi.org/10.1038/ncomms13043

Pack, M. A., Xu, X., Lupascu, M., Kessler, J. D., & Czimczik, C. I. (2015). A rapid method for preparing low volume CH4 and CO2 gas samples for 14C AMS analysis. *Organic Geochemistry*, *78*, 89-98. https://doi.org/10.1016/j.orggeochem.2014.10.010

Phillips, D. L., & Gregg, J. W. (2003). Source partitioning using stable isotopes: coping with too many sources. Oecologia, 136(2), 261-269.

Prėskienis, V., Laurion, I., Bouchard, F., Douglas, P. M., Billett, M. F., Fortier, D., & Xu, X. (2021). Seasonal patterns in greenhouse gas emissions from lakes and ponds in a High Arctic polygonal landscape. *Limnology and Oceanography*.

Raymond, P. A., McClelland, J. W., Holmes, R. M., Zhulidov, A. V., Mull, K., Peterson, B. J., ... & Gurtovaya, T. Y. (2007). Flux and age of dissolved organic carbon exported to the Arctic Ocean: A carbon isotopic study of the five largest arctic rivers. *Global Biogeochemical Cycles, 21*(4). https://doi.org/10.1029/2007GB002934

Schuur, E. A. G., McGuire, A. D., Schädel, C., Grosse, G., Harden, J. W., Hayes, D. J., … Vonk, J. E. (2015). Climate change and the permafrost carbon feedback. *Nature*, *520*(7546), 171–179. https://doi.org/10.1038/nature14338

Skoog, A. C., & Arias-Esquivel, V. A. (2009). The effect of induced anoxia and reoxygenation on benthic fluxes of organic carbon, phosphate, iron, and manganese. *Science of the total environment*, *407*(23), 6085-6092. https://doi.org/10.1016/j.scitotenv.2009.08.030

Smith, S. L., Romanovsky, V. E., Lewkowicz, A. G., Burn, C. R., Allard, M., Clow, G. D., ... & Throop, J. (2010). Thermal state of permafrost in North America: a contribution to the international polar year. *Permafrost and Periglacial Processes*, *21*(2), 117-135. https://doi.org/10.1002/ppp.690

Spencer, R. G. M., P. J. Mann, T. Dittmar, T. I. Eglinton, C. McIntyre, R. M. Holmes, N. Zimov, and A. Stubbins (2015), Detecting the signature of permafrost thaw in Arctic rivers, *Geophys. Res. Lett., 42*, 2830–2835, doi:10.1002/ 2015GL063498.

Stepanenko, V. M., Machul'Skaya, E. E., Glagolev, M. V., & Lykossov, V. N. (2011). Numerical modeling of methane emissions from lakes in the permafrost zone. *Izvestiya, Atmospheric and Oceanic Physics, 47*(2), 252-264. https://doi.org/10.1134/S0001433811020113

Summons, R. E., Franzmann, P. D., & Nichols, P. D. (1998). Carbon isotopic fractionation associated with methylotrophic methanogenesis. *Organic Geochemistry*, *28*(7-8), 465-475. https://doi.org/10.1016/S0146-6380(98)00011-4

Tank, S. E., Vonk, J. E., Walvoord, M. A., McClelland, J. W., Laurion, I., & Abbott, B. W. (2020). Landscape matters: Predicting the biogeochemical effects of permafrost thaw on aquatic networks with a state factor approach. Permafrost and Periglacial Processes, 31(3), 358–370. https://doi.org/10.1002/ppp.2057

Vallée, S., & Payette, S. (2007). Collapse of permafrost mounds along a subarctic river over the last 100 years (northern Quebec). *Geomorphology*, *90*(1-2), 162-170. https://doi.org/10.1016/j.geomorph.2007.01.019

Vigneron, A., Lovejoy, C., Cruaud, P., Kalenitchenko, D., Culley, A., & Vincent, W. F. (2019). Contrasting winter versus summer microbial communities and metabolic functions in a permafrost thaw lake. *Frontiers in microbiology*, *10*, 1656. https://doi.org/10.3389/fmicb.2019.01656

Vincent, W. F., Lemay, M., & Allard, M. (2017). Arctic permafrost landscapes in transition: towards an integrated Earth system approach. *Arctic Science*, *3*(2), 39-64. https://doi.org/10.1139/as-2016-0027

Walter, K.M., Zimov, S.A., Chanton, J.P., Verbyla, D. and Chapin, F.S., (2006). Methane bubbling from Siberian thaw lakes as a positive feedback to climate warming. *Nature,* 443(7107), pp.71-75.

Walter Anthony, K., Daanen, R., Anthony, P., Schneider Von Deimling, T., Ping, C. L., Chanton, J. P., & Grosse, G. (2016). Methane emissions proportional to permafrost carbon thawed in Arctic lakes since the 1950s. *Nature Geoscience*, *9*(9), 679–682. https://doi.org/10.1038/ngeo2795

Wang, J. J., Lafrenière, M. J., Lamoureux, S. F., Simpson, A. J., Gélinas, Y., & Simpson, M. J. (2018). Differences in Riverine and Pond Water Dissolved Organic Matter Composition and Sources in Canadian High Arctic Watersheds Affected by Active Layer Detachments. *Environmental Science and Technology*, *52*(3), 1062–1071. https://doi.org/10.1021/acs.est.7b05506

Wang, Z., Roulet, N. (2017). Comparison of plant litter and peat decomposition changes with permafrost thaw in a subarctic peatland. *Plant Soil 417*, 197–216 . https://doi.org/10.1007/s11104-017-3252-7

Whiticar, M. J. (1999). Carbon and hydrogen isotope systematics of bacterial formation and oxidation of methane. *Chemical Geology*, *161*(1), 291–314. https://doi.org/10.1016/S0009-2541(99)00092-3

Wik, M., Thornton, B. F., Bastviken, D., MacIntyre, S., Varner, R. K., & Crill, P. M. (2014). Energy input is the primary controller of methane bubbling in subarctic lakes. *Geophysical Research Letters*, *41*(2), 555-560.

Wild, B., Andersson, A., Bröder, L., Vonk, J., Hugelius, G., McClelland, J. W., … Gustafsson, Ö. (2019). Rivers across the Siberian Arctic unearth the patterns of carbon release from thawing permafrost. *Proceedings of the National Academy of Sciences*, *116*(21), 10280–10285. https://doi.org/10.1073/PNAS.1811797116

Zhang, J., Quay, P. D., & Wilbur, D. O. (1995). Carbon isotope fractionation during gas-water exchange and dissolution of CO2. *Geochimica et Cosmochimica Acta*, *59*(1), 107-114.

Zimov, S. A., Voropaev, Y. V., Semiletov, I. ., Davidov, S. P., Prosiannikov, S. F., Chapin III, F. S., … Tyler, S. (1997). North Siberian Lakes: A Methane Source Fueled by Pleistocene Carbon. *Science*, *277*(5327), 800–802. https://doi.org/10.1126/science.277.5327.800

Quebec

Hudson Bay

KWK

SAS

Lithalsa lakes

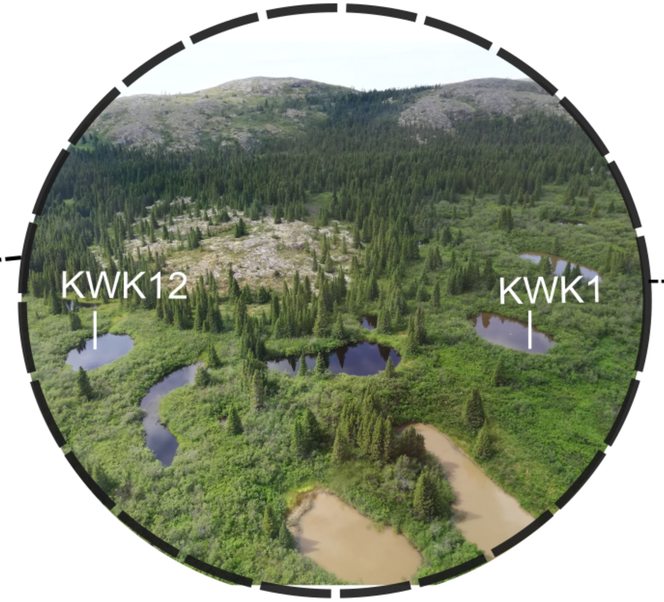

55°19’50.7”N
77°30’15.9”W

Summer

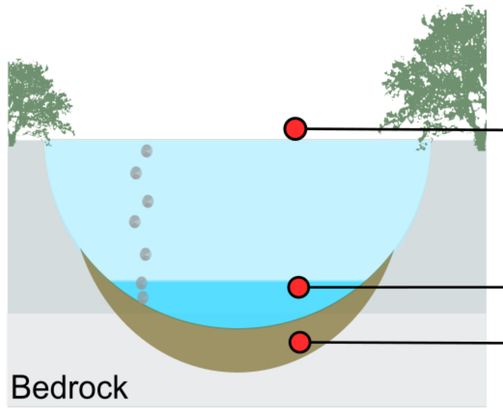

Diffusive fluxes
(mmol m^{-2} d^{-1})
CH_4: 0.47 ± 0.33
CO_2: 20.2 ± 7.1

Anoxic below 1.5 m

< 2% carbon in sediments

SAS river

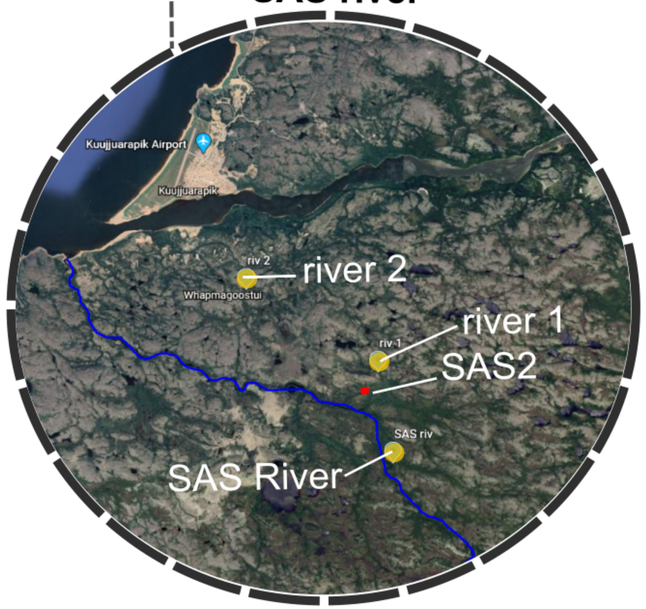

55°12’35.9”N
77°41’05.1”W

Palsa Lakes

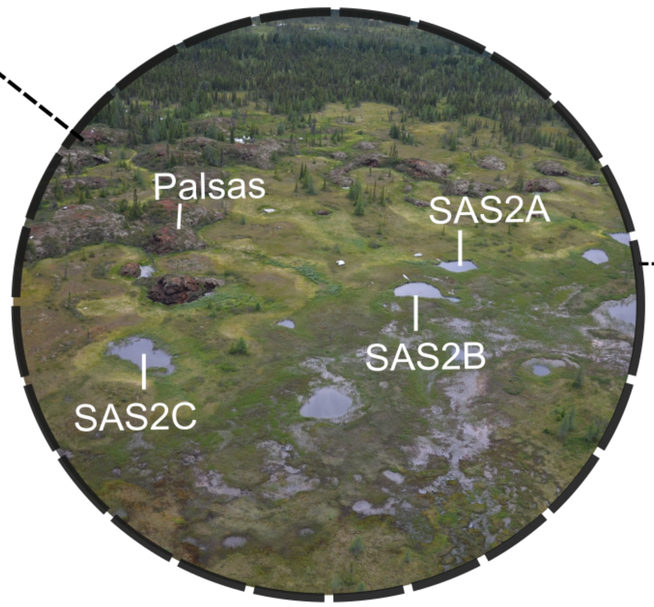

55°13’36.7”N
77°41’44.1”W

Summer

Diffusive fluxes
(mmol m^{-2} d^{-1})
CH_4: 1–10
CO_2: 40–242

Anoxic below 0.5 m

>24% carbon in sediments

Winter

Limited gas exchange and hydrological transport

Anoxic

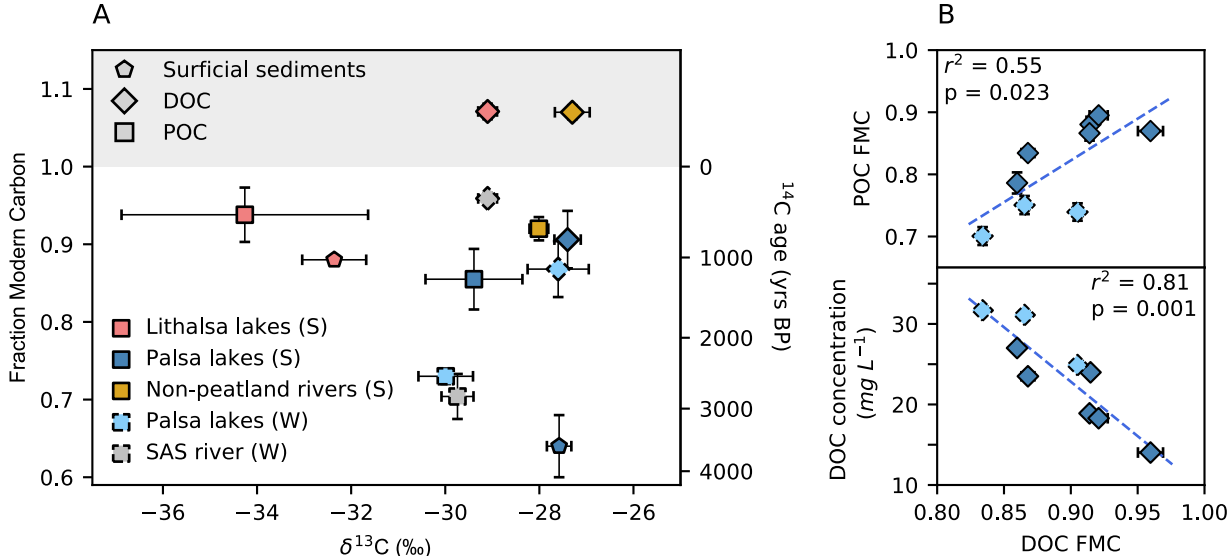
A
Surficial sediments
DOC
POC
Lithalsa lakes (S)
Palsa lakes (S)
Non-peatland rivers (S)
Palsa lakes (W)
SAS river (W)
Fraction Modern Carbon
^{14}C age (yrs BP)
δ^{13}C (‰)
B
r^2 = 0.55
p = 0.023
POC FMC
r^2 = 0.81
p = 0.001
DOC concentration (mg L^{-1})
DOC FMC

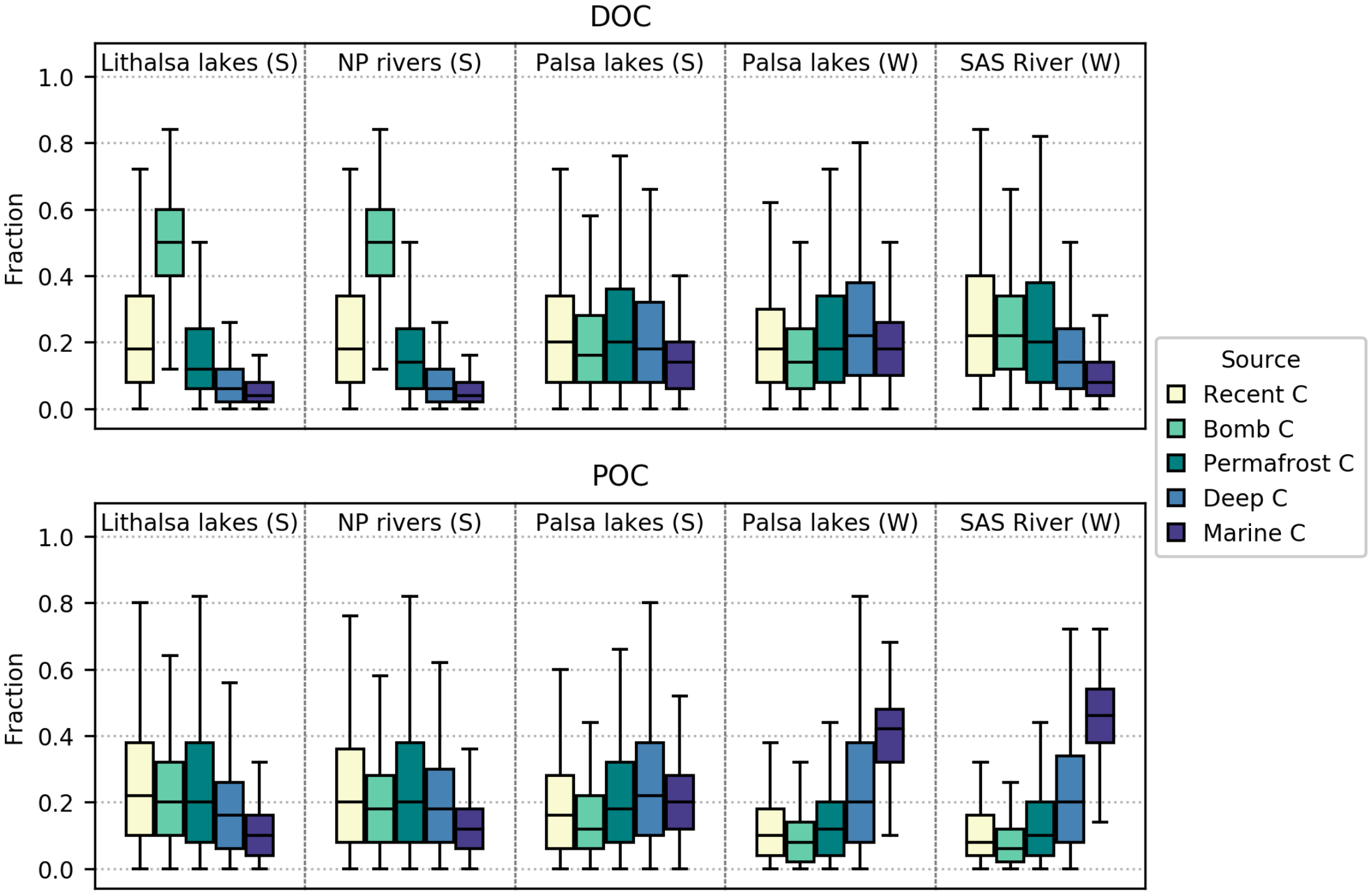
DOC
Lithalsa lakes (S)
NP rivers (S)
Palsa lakes (S)
Palsa lakes (W)
SAS River (W)
Fraction
1.0
0.8
0.6
0.4
0.2
0.0
POC
Lithalsa lakes (S)
NP rivers (S)
Palsa lakes (S)
Palsa lakes (W)
SAS River (W)
Fraction
1.0
0.8
0.6
0.4
0.2
0.0
Source
Recent C
Bomb C
Permafrost C
Deep C
Marine C

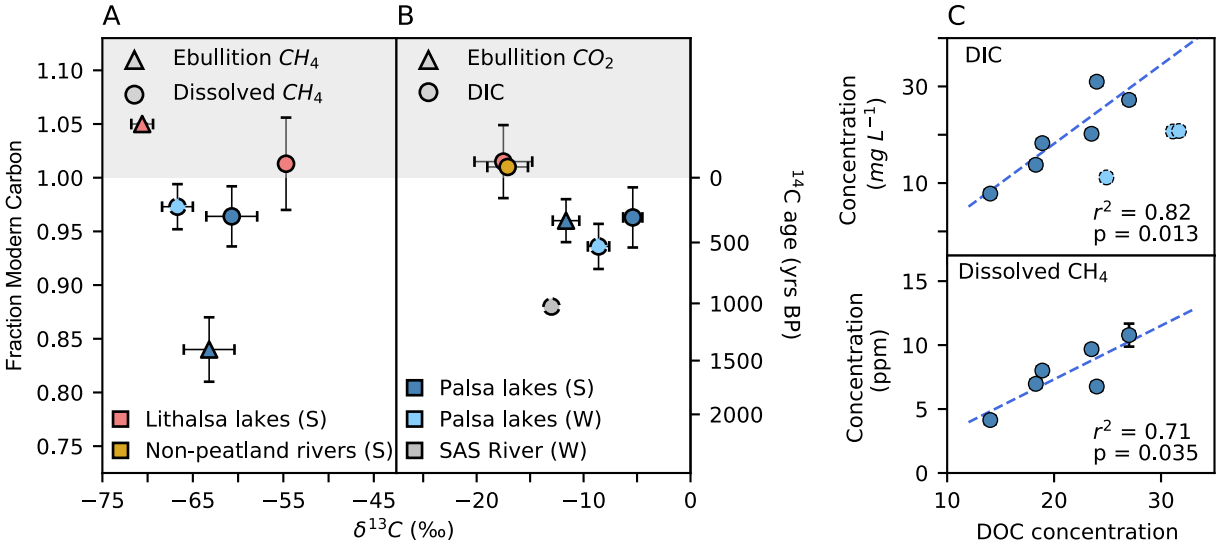
A
B
C
Ebullition CH_4
Dissolved CH_4
Ebullition CO_2
DIC
Lithalsa lakes (S)
Non-peatland rivers (S)
Palsa lakes (S)
Palsa lakes (W)
SAS River (W)
Fraction Modern Carbon
$\delta^{13}C$ (‰)
^{14}C age (yrs BP)
Concentration ($mg\ L^{-1}$)
r^2 = 0.82
p = 0.013
Concentration (ppm)
r^2 = 0.71
p = 0.035
DOC concentration

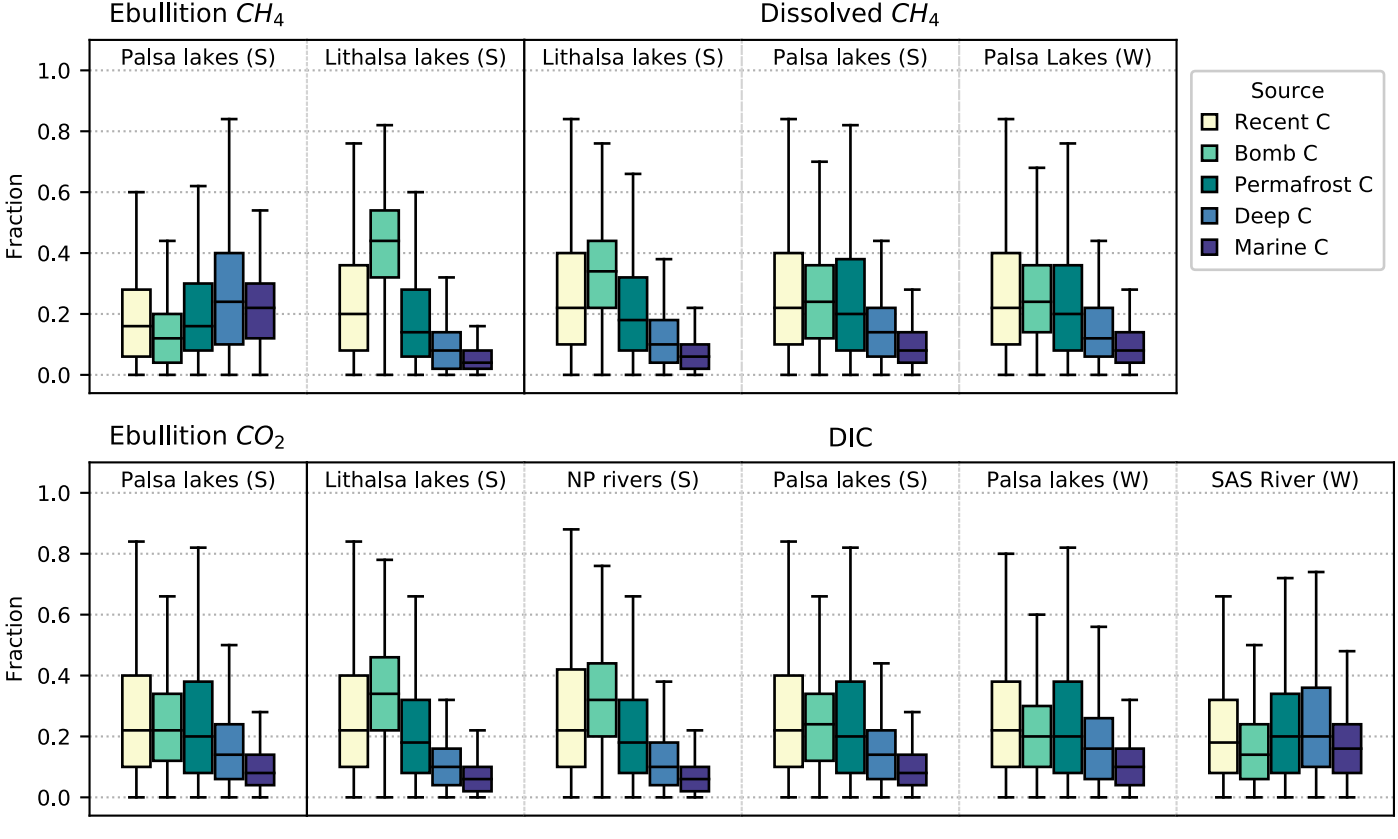
Ebullition CH_4
Dissolved CH_4
Palsa lakes (S)
Lithalsa lakes (S)
Lithalsa lakes (S)
Palsa lakes (S)
Palsa Lakes (W)
Source
Recent C
Bomb C
Permafrost C
Deep C
Marine C
Fraction
1.0
0.8
0.6
0.4
0.2
0.0
Ebullition CO_2
DIC
Palsa lakes (S)
Lithalsa lakes (S)
NP rivers (S)
Palsa lakes (S)
Palsa lakes (W)
SAS River (W)
Fraction
1.0
0.8
0.6
0.4
0.2
0.0